ELECTRICAL RESISTIVITY CHANGES IN TUFFS

by

Carolyn Alexandria Morrow

S.B., Massachusetts Institute of Technology

(1978)

SUBMITTED IN PARTIAL FULFILLMENT

OF THE REQUIREMENTS FOR THE

DEGREE OF

MASTER OF SCIENCE

at the

MASSACHUSETTS INSTITUTE OF TECHNOLOGY

September, 1979

Signature of Author.....
Department of Earth and Planetary Sciences,
September, 1979

Certified by.....
Thesis Supervisor

Accepted by.....
Chairman, Department Committee on Graduate Students

ABSTRACT

ELECTRICAL RESISTIVITY CHANGES IN TUFFS

by

Carolyn Alexandria Morrow

Submitted to the Department of Earth and Planetary Sciences on August 28 , 1979 in partial fulfillment of the requirements for the degree of Master of Science.

Samples of northern California tuffs were stressed while simultaneously measuring electrical resistance changes to investigate a phenomenon observed by Yamazaki on similar rocks from Japan. Resistance decreased substantially at low strain values for partially saturated samples. Strain was amplified between 10^3 and 10^5 by the associated change in electrical resistance.

The process was repeatable and recoverable in the tuffs unlike the behavior of other rock types. The principal factors involved were porosity, Young's modulus and degree of saturation.

A method is described to quickly sort out the electrically amplifying tuffs from those that are not, as a first step in locating a field site where this phenomenon could be used as an earthquake monitoring technique.

Thesis Supervisor: William F. Brace
Professor of Geology

TABLE OF CONTENTS

LIST OF FIGURES

LIST OF TABLES

ACKNOWLEDGMENTS

I would like to thank William F. Brace for his support and advice throughout this work. Charles Chesterman of the California Bureau of Mines and Garniss Curtis of the University of California at Berkeley aided in the location and collection of samples. Michael Coln was very helpful in improving the electrical measuring techniques, and in typing this thesis.

CHAPTER I

Introduction

In 1965 Yamazaki called attention to dramatic electrical resistivity changes thought to be caused by earth tides. Resistivity variations a thousand times larger than the tidal strain were recorded in a cave near Tokyo, Japan. Although the tidal origin is still disputed Madden, [1978], Yamazaki subsequently confirmed in the laboratory [1965, 1966] the unusual electrical sensitivity to strain of the particular tuffaceous rocks where the field observations were first made. Others have shown that resistivity of rocks changes with stress (Parkhomenko [1967], Brace and Orange [1968], for example), but generally the changes were but a small fraction of those noted by Yamazaki, particularly in porous rocks [Brace 1974].

The electrical effects reported by Yamazaki were limited to tuffaceous rocks, partially saturated and at very low stresses. Because of the potential application to crustal deformation studies or to earthquake prediction (Rikitake and Yamazaki [1969]), it seemed worthwhile to extend his work, not only to other rocks, but to a wider range of conditions. Tuffaceous sandstone showed a weaker effect than lapilli tuff [Yamazaki 1966]. Would other sandstones be similar? What is the optimum mineralogy,

porosity, saturation and stress level? Do appropriate rocks exist near active fault zones in the United States? Even if they do not, the mechanism of this fascinating effect needs to be explained. How can resistivity in a partially saturated highly porous rock change so dramatically in a reversible way?

To explore such questions, a laboratory experiment was designed which would attain the conditions of stress, saturation and would include rock types similar to those studied by Yamazaki. Since the field site was located in a tuff cave with electrodes affixed to the floor and walls, an unconfined compression test best approximated the in situ stress state. In the compression tests, stress, strain and electrical resistance were simultaneously measured to a maximum stress of 6 MPa. This stress was chosen to avoid permanent damage to the weak tuffs and sandstones studied. A low stress cycle would ensure repeatable elastic behavior and perhaps simulate tidal earth loads and certain tectonic stresses.

Research was carried out in four distinct phases. These were: a) a study of the electrical properties of sandstones and tuffs from Nevada and Montana to verify and further investigate Yamazaki's findings. Preliminary results were very promising, but the details were vaguely

understood. Nevertheless, the next step was b) sample collection of tuffs near active California faults, since a major goal was the location of sites in the United States where tuffs could be used in earthquake prediction. Then c) a rapid approximate method was devised to find which of the California rocks had more pronounced electrical properties, and d) several of these tuffs were investigated in detail under a more complete range of saturations to answer some of the basic questions mentioned above.

Due to the more comprehensive nature of the California study, these results are presented as the principal text of this thesis. The work on sandstones and the Nevada/Montana tuffs are described in Appendix A. There are a few places where these data are included with the results of the California rocks, particularly for completeness and comparison of rock types. These spots are noted and referenced.

CHAPTER II

Rocks Studied

Sampling

With the help of state maps and local geologists, several tuff sites were located in norther California. The principal locations were (a) volcanics of the Pinnacles National Monument, adjacent to the San Andreas fault, (b) the Berkeley Hills volcanics, next to the Hayward fault, and (c) the Napa, Somona and Cotati valleys, which are cut by several lesser faults. In many of these areas, a number of distinctive tuff deposits are exposed, each of which was sampled. Sampling was conducted in the dry season (July), from fresh surface outcrops, with care taken to preserve natural water content.

With the large number of samples involved, (from over a dozen sites), it was impossible to do a detailed study of each locality. Therefore a quick test was devised to sort out the more electrically sensitive rocks. This was called the "chunk test", in reference to the hand specimen size chunks of rocks used rather than machined samples. The intent of the test was not to produce accurate quantitative data, but quickly order the rocks in terms of electrical properties. Details are described in Appendix B. From the

results of the chunk tests, six tuffs from the Berkeley Hills and Napa valley were chosen for more thorough study (Table 2.1). A sandstone (Berea) is also included in the table. Detailed results of other sandstones can be found in Appendix A.

Rock Descriptions

Tuffs are the products of explosive volcanic eruptions. Ash, crystals, glass and rock fragments consolidate into a porous rock. Carossi [1960] gives a comprehensive description of tuff petrology and vitroclastic texture.

The six tuffs listed in Table 2.1 represent the three general catagories of tuffs. SZT and RTT are lithic tuffs, composed mostly of rock fragments welded together by a tuffaceous matrix. GPT and DPR fall into the catagory of crystal tuffs, which contain a large percentage of phenocrysts. Finally, SHR and SIL are vitric tuffs, composed mostly of fine-grained glassy groundmass.

In the descriptions of Table 2.1 (as seen in thin section), the amount of breakdown of the unstable glass to clay minerals and zeolites was estimated, as these samples were not analyzed by X-ray techniques.

Study of fresh fracture surfaces with the scanning electron microscope revealed a wide range of internal structures, reflecting tuff type. The glassy specimens, with little recrystallization of the groundmass had numerous very small pores (0.5 microns) caused by gas bubbles. SIL was the most notable example of this type. With increasing

recrystallization, pores and passageways evidently became larger, to a maximum of around 50 microns, although precise determination of pore size, glass content and mineral phases was difficult from fracture surface micrographs. An attempt was made to study pore geometry from polished surfaces using the ion thinning technique described in Sprunt and Brace [1974]. These results were largely unsuccessful as the tuffs were very soft and did not thin uniformly.

Table 2.1 Rock Descriptions of Selected California Tuffs

Sample	Location	Porosity (%)	Young's Mod., GPa	Description
DPR	Deer Park Rd. St. Helena, Napa County	17.9	3.5	20% plagioclase and sanidine phenocrysts 80% fine grain reworked groundmass, welded banding and flow textures
SHR	St. Helena Road., Sonoma Co.	37.2	2.2	10% phenocrysts including: 8% plagioclase 2% fractured quartz X % lithic fragments 90% groundmass: 30% glassy lenses & shard structures 30% recrystallized radial zeolites 30% fine grained groundmass
SZT	Siesta Formation zeolite tuff Berkeley Hills	17.1	3.3	80% basaltic lithic fragments 5% plagioclase- very fractured 15% zeolitized matrix
RTT	Round Top Hill Berkeley Hills	3.7	12.5	60% basalt fragments 5% crystalline quartz X % zeolitized plagioclase 35% reworked glass, clay and zeolites
GPT	Grizzly Peak Berkeley Hills	10.7	10.0	30% phenocrysts: angular fragments, variable size, includes: 20% plagioclase 5% quartz few % biotite 10% lithic fragments 60% groundmass, including iron rich montmorillonite, isolated areas of banded texture

Sample	Location	Porosity* (%)	Young's Mod., GPa	Description
SIL	Silverado Trail, Napa County	35.6	2.4	65% glass 30% pumice fragments few % quartz and plagioclase phenocrysts
Berea sandstone	Ohio, W. Virginia	17.2	6.5	Orthoquartzite: 95% quartz & chert 5% feldspar

*Porosities were determined using the immersion method described in Brace, Orange and Madden [1965].

CHAPTER III

Experimental Procedure

Rock samples were machined into cylindrical cores 2.5 cm in diameter by 5 cm long. BLH strain gauges (FA-50-12-S6), oriented along the cylindrical axis, recorded linear strain. An oil pressure piston device was used to stress the samples in unconfined uniaxial compression up to an axial stress of 6 MPa as shown schematically in Figure 3.1. Lead electrode sheets, 1.3 mm in thickness were attached to either end of the sample to form one side of a Wheatstone bridge. A detailed description of resistance measurement techniques can be found in Appendix D. The sample and electrodes were insulated from the piston and load cell by a 0.1 mm layer of Pallflex teflon.

Electrical resistance measurements were taken at stress levels of 0, 0.2, 0.5, 1, 2, 4, and 6 MPa for both increasing and decreasing stresses. Sampling was more frequent at the lower stresses as the most change was expected when the sample first began to strain. In all cases a source voltage across the rock of 10 Hz AC was used to minimize the frequency effects due to rock capacitance at high resistance values.

The pore fluid used was 35 ohm-meter tap water. Saturation level was determined by averaging the weights of the sample both before and after each run. For low saturation, the variation was at most 1 percent, for higher saturation it reached 5 percent. Stress and strain measurements were accurate to 5 percent. The absolute resistance was known to 20 percent, and relative changes in resistance were accurate to 5 percent.

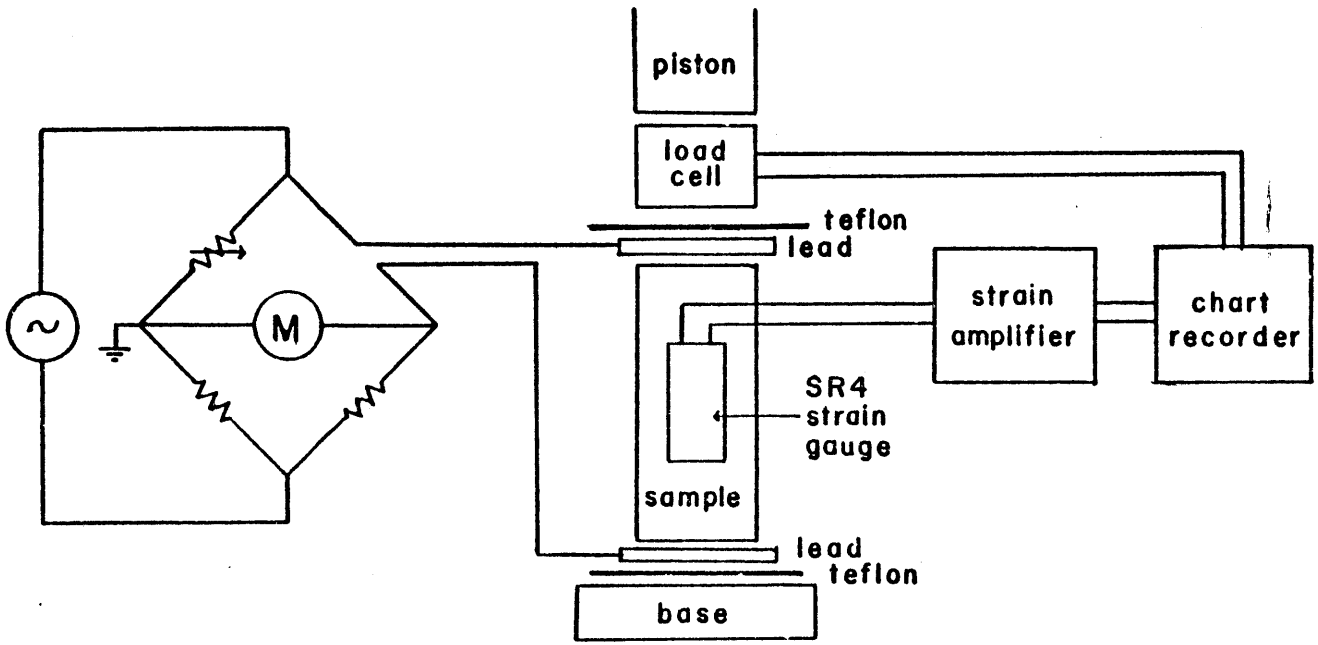

Figure 3.1 Experimental Apparatus

CHAPTER IV

Observations

Stress-Strain Behavior

Stress-strain behavior in tuffs was highly dependent on porosity, previous stress history and time factors. Some samples showed a permanent change in the first stress cycle, as either a permanent strain or an increase in the modulus. Succeeding cycles were all nearly identical and fairly linear on loading and unloading (Figure 4.1a). Other samples were less recoverable and also changed with time after a loading cycle, as seen for instance with DPR (Figure 4.1b). On the left is the initial trace. Then, immediately after the first stress cycle, the sample had become stiffer (center trace). The trace on the right was taken several days later when the sample had relaxed. The stress-strain curves for sandstone were similar in shape to those of DPR. Young's modulus was closely related to porosity (Figure 4.2); the more porous rocks tended to be less stiff.

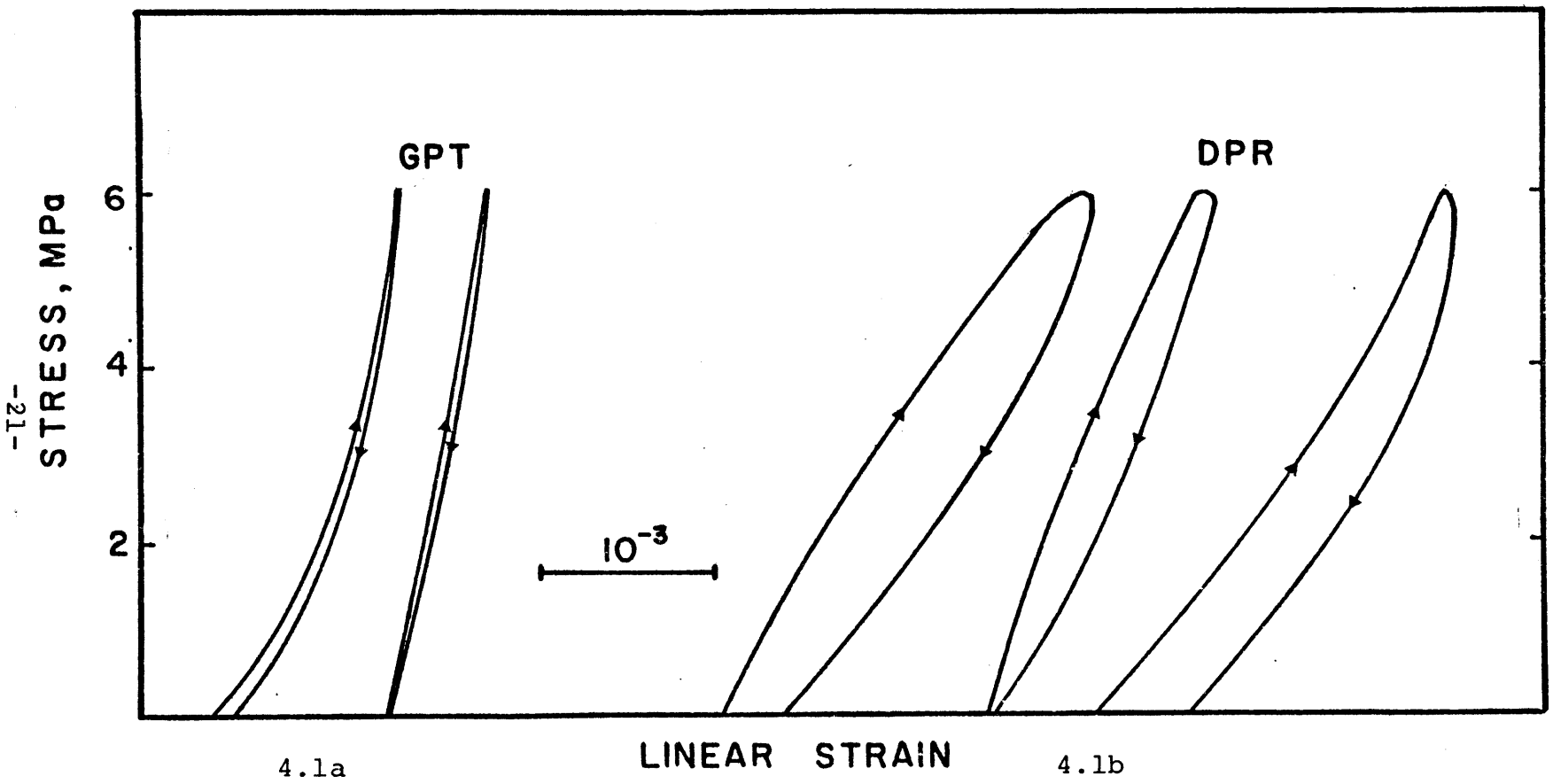

Figure 4.1 Typical stress-strain curves, GPT and DPR

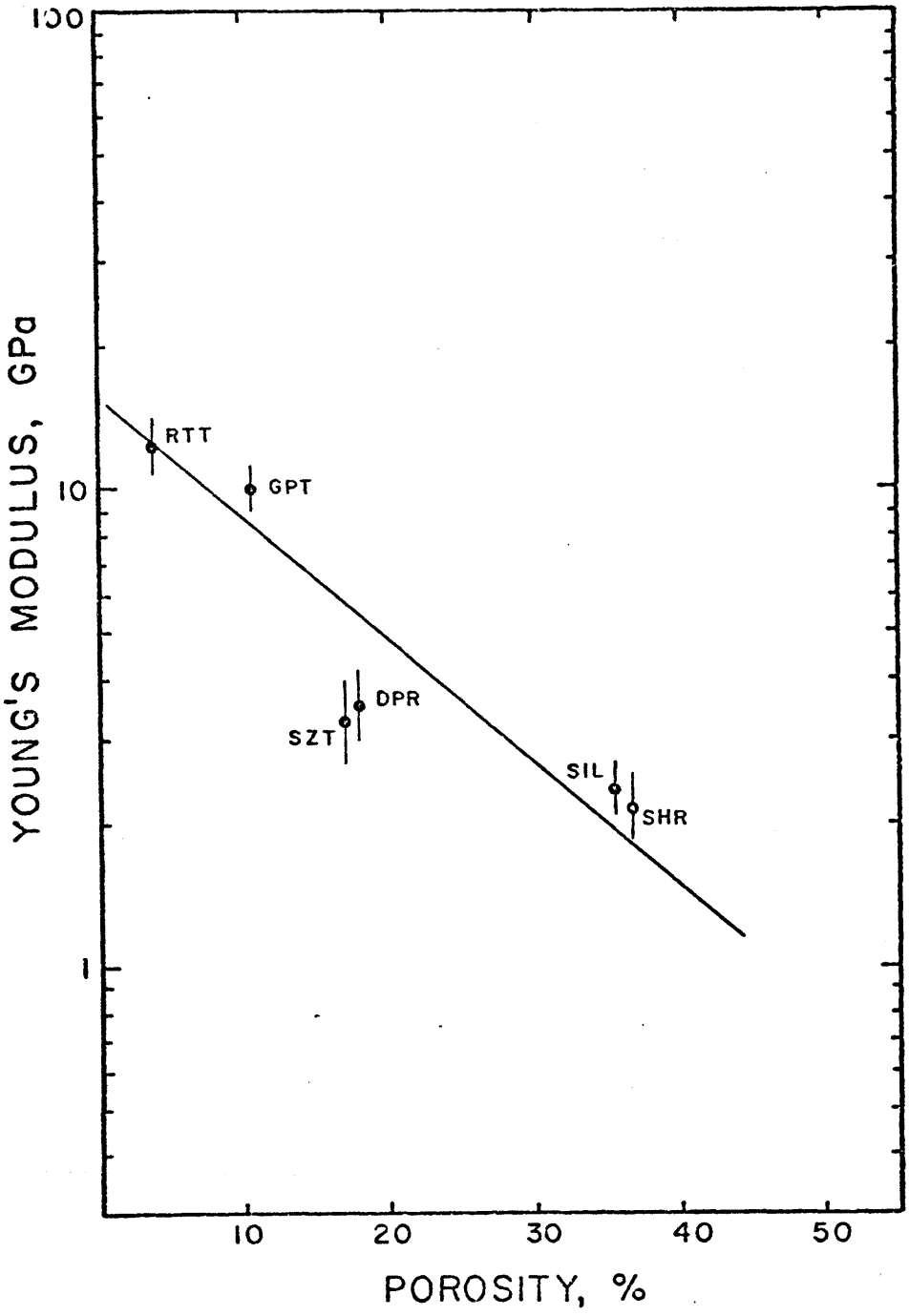

Figure 4.2 Young's Modulus of tuff samples vs. porosity

Electrical Changes with Stress

Grizzly Peak tuff (GPT) and Berea sandstone showed changes in resistance with stress that were typical of their respective rock types (Figure 4.3). Data for the other samples can be found in the appendices. Unloading curves consistently fell below loading curves; electrically GPT recovered nearly completely, the sandstone hardly at all. Recoverability varied somewhat among the tuffs. Once loaded, resistance of the sandstone changed little with stress, either upon unloading, or during subsequent cycles (Figure 4.3).

The sole observation of resistive effects in crystalline rocks [Brace and Orange, 1968] suggests that they behave like sandstone when partially saturated. Resistivity rapidly decreased with stress for Westerly granite at 45 percent saturation. Upon unloading and subsequent loading, resistivity changes were quite small and in the same direction as for saturated rocks, that is, in the reverse direction to the changes seen in the tuffs.

Returning to the porous rocks of this study, resistivity predictably decreased with saturation; a typical value was 10^7 ohm-meters at low saturation, and 10^3 ohm-meters at high values. Also, changes in resistance

(or equivalently, resistivity) with stress depended on saturation. Silverado Trail tuff (SIL) was typical: at high saturation $\Delta\rho/\rho$ changed little (Figure 4.4). As water content decreased the slopes became steeper and the change in resistance was larger. At some value of saturation the trend was reversed, and changes in resistance were small again.

A convenient way to compare this effect among different samples is to define a quantity called the amplification factor, $(\Delta\rho/\rho)_{\varepsilon-4}$, namely the slope of the $\Delta\rho/\rho$ plot at a strain of 10^{-4}. Higher amplification factors indicate more sensitivity to earth strain. The values measured ranged between 10^3 and 10^5.

Amplification factor depended on saturation as shown in Figure 4.5. The amplification increased with decreasing saturation to a peak value and then fell off. The peak saturation is significant in that it corresponds to the highest sensitivity to strain.

As strain is related to Young's modulus through Hooke's Law, peak saturation should be dependent on the modulus. This was indeed the case (Figure 4.6). Stiffer rocks required more conducting fluid to reach optimum sensitivity (highest amplification factor). Variations in Young's

modulus in the tuffs was primarily related to porosity (Figure 4.2), therefore porosity and peak saturation must exhibit a strong correlation (Figure 4.7). This can be used to predict the water contents necessary for high amplification, given porosity data.

Porosity was thus a controlling parameter for both the amplification factor and the peak saturation. Less porous rocks were better able to amplify strain (Figure 4.8), but required higher water content to do so (Figure 4.9). This was predominantly a result of the variations in rock stiffness and its effects on cracks, as discussed later. There was no constant volume of water in the rocks as might have been inferred from the inverse slopes of Figures 4.8 and 4.9.

Table 4.1 lists the amplification factors for each sample at several saturations, and Table 4.2 contains a summary of the important physical parameters of each rock. The graphs from which these numbers were derived are compiled in Appendix C.

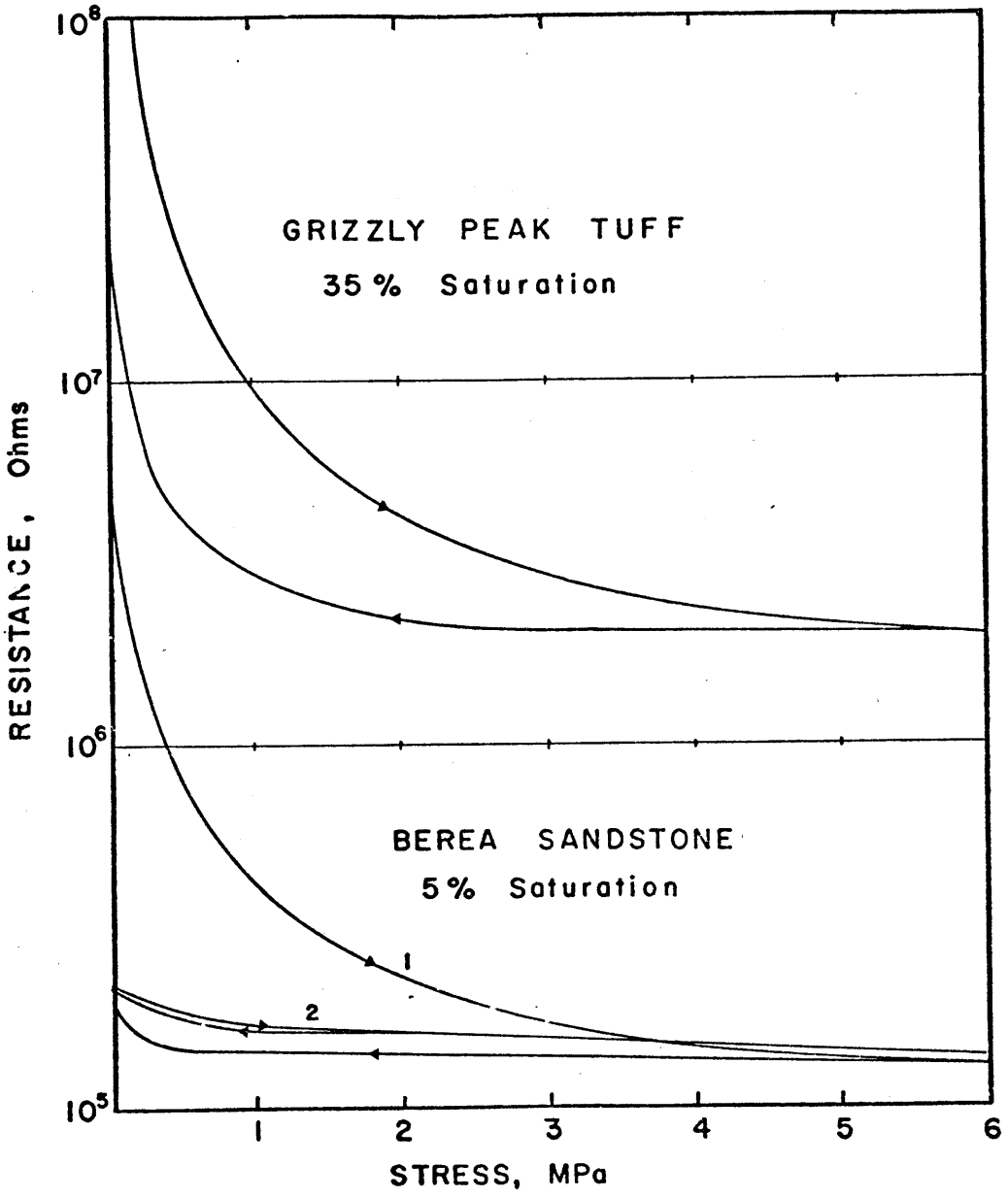

Figure 4.3 Change in electrical resistance with stress of the Grizzly Peak tuff and Berea sandstone

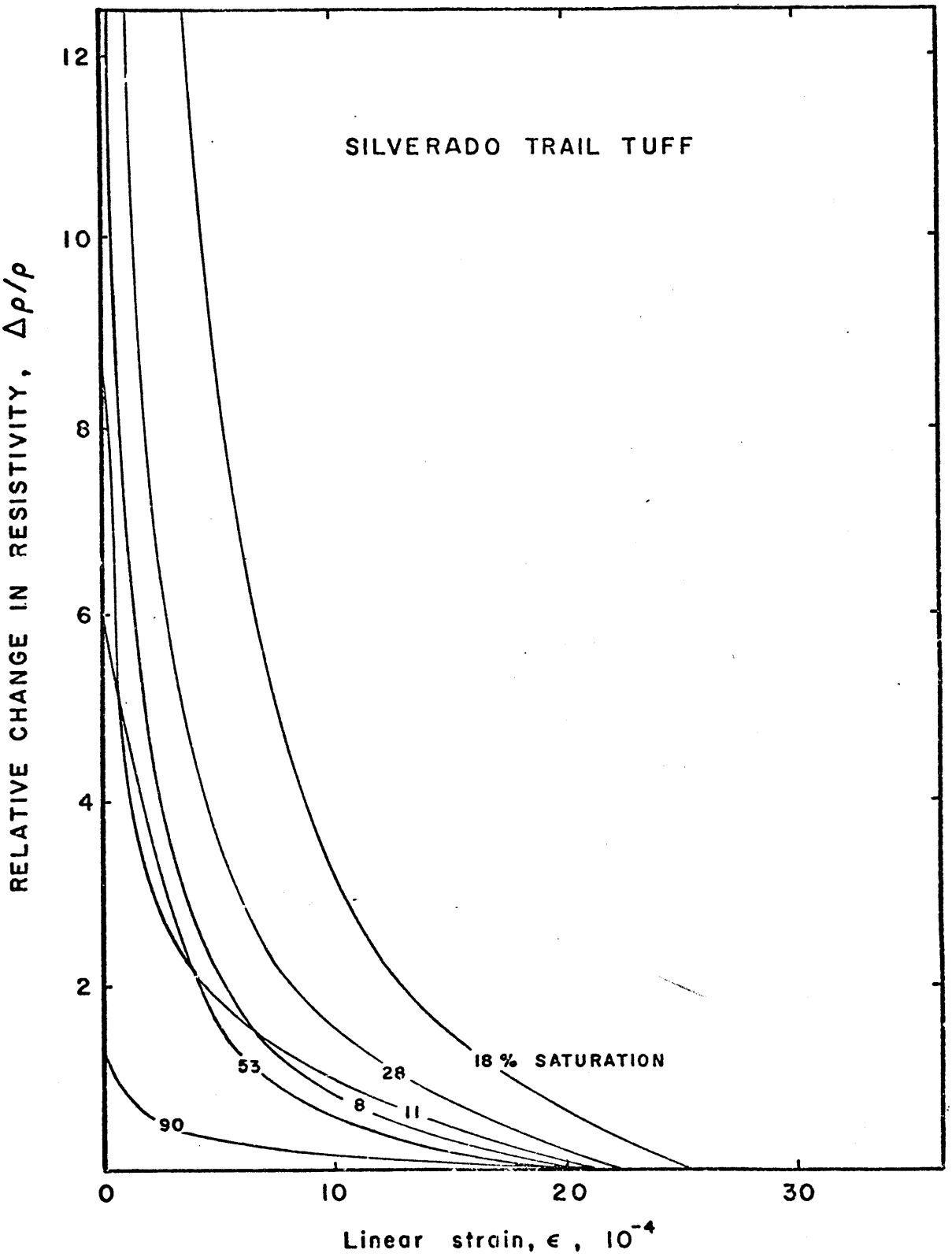

Figure 4.4 Relative change in resistivity with strain, SIL

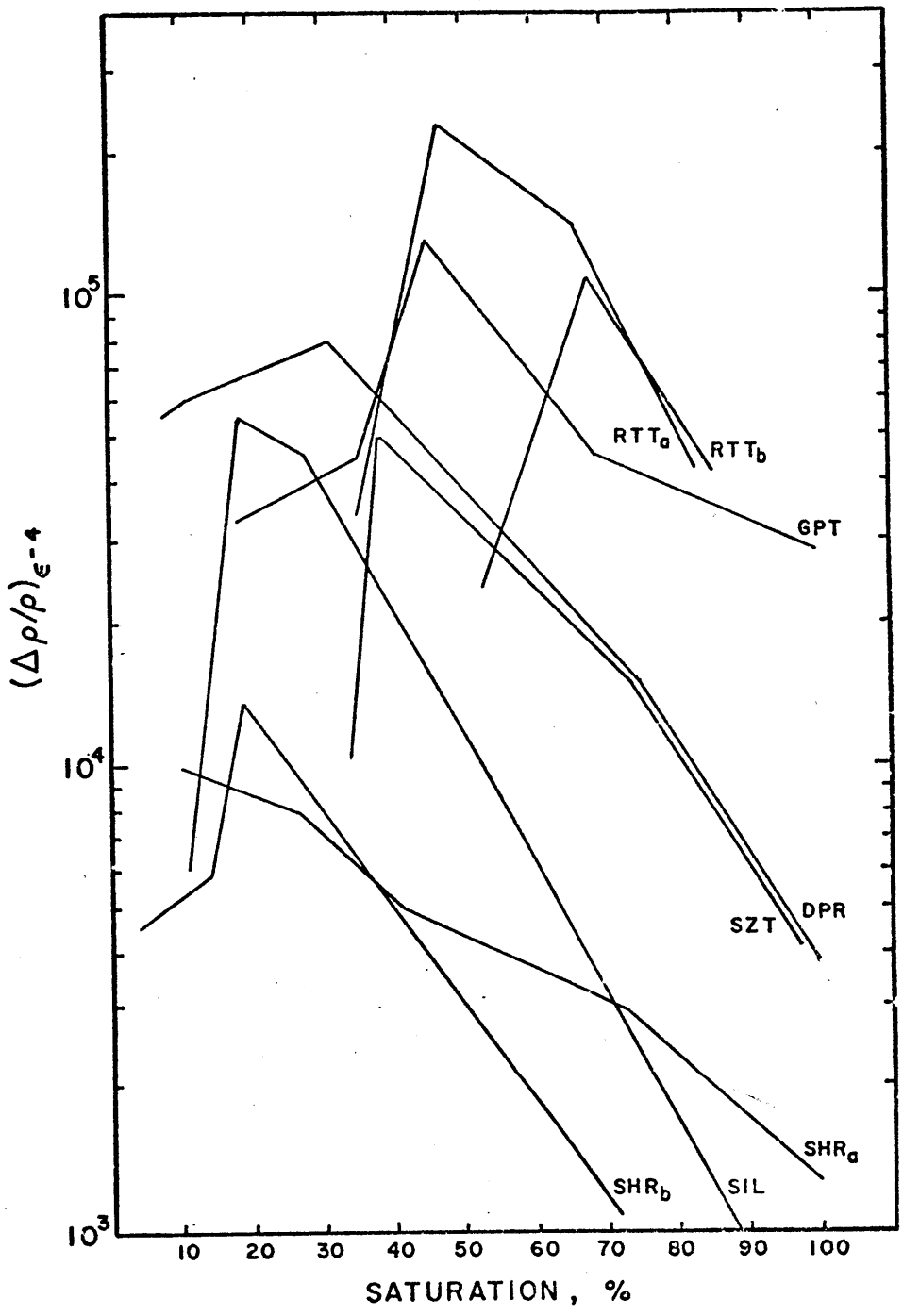

Figure 4.5 Amplification factor vs. saturation

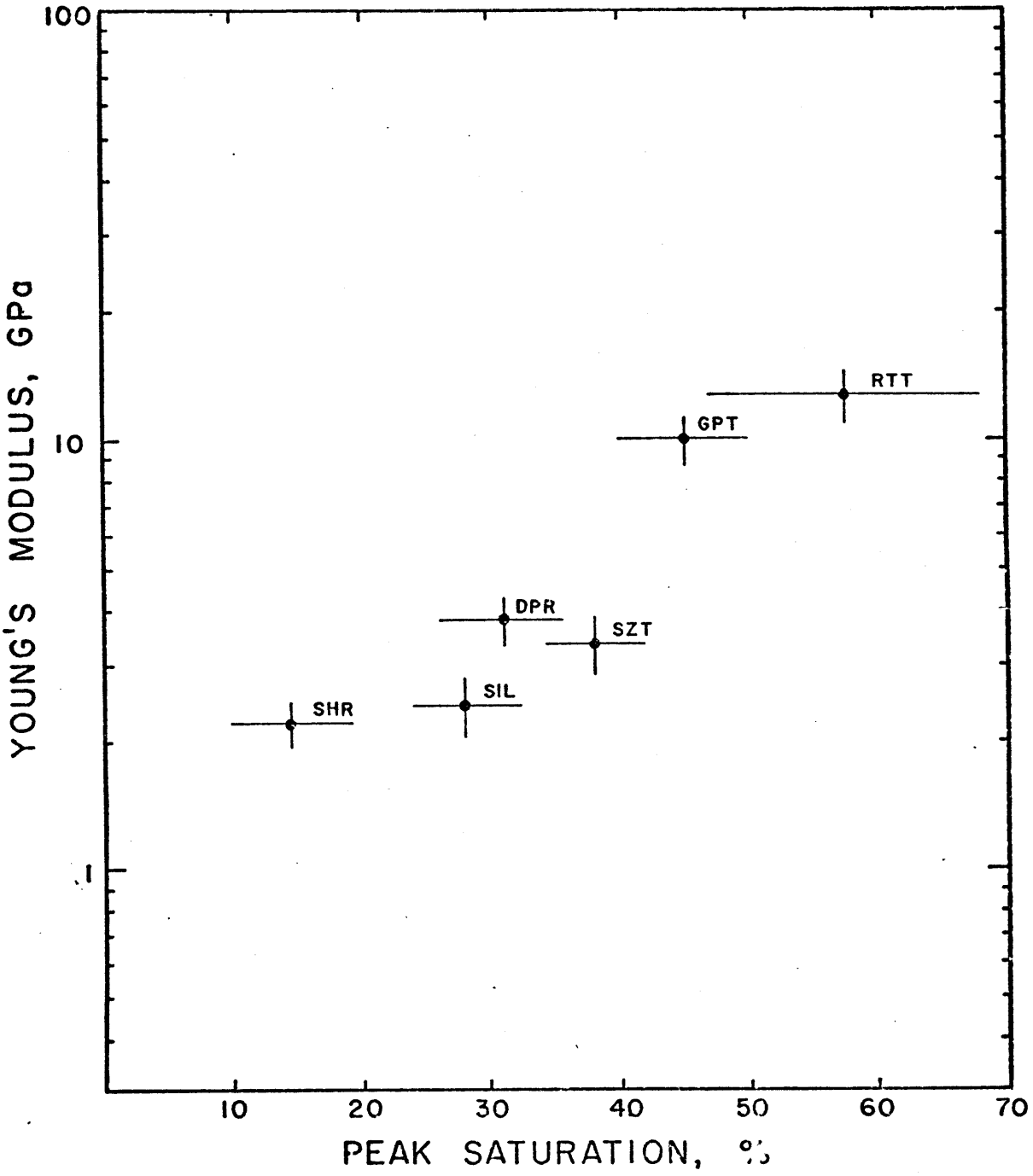

Figure 4.6 Relation of Young's modulus to saturation at maximum amplification (peak saturation)

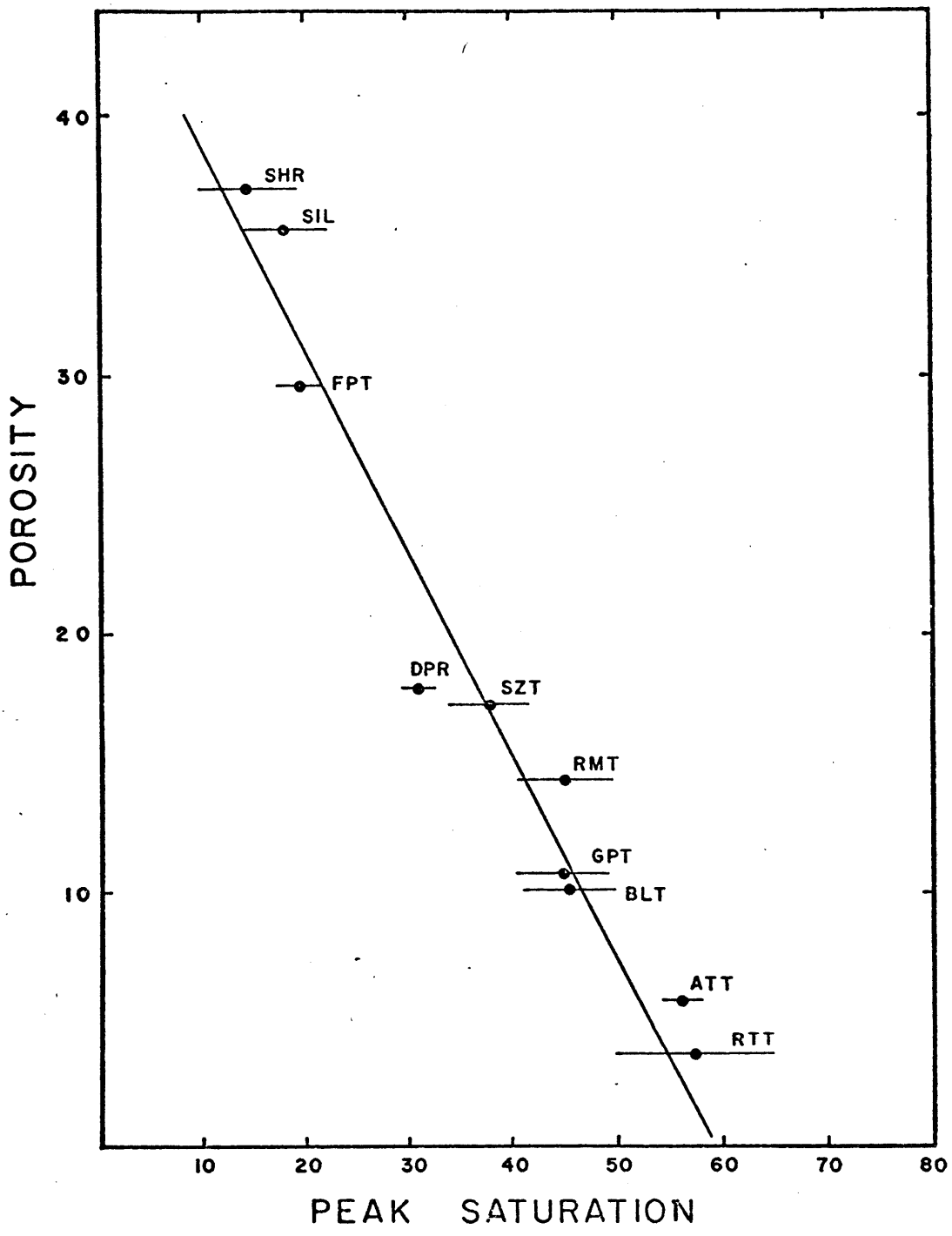

Figure 4.7 Porosity of tuffs vs. peak saturation

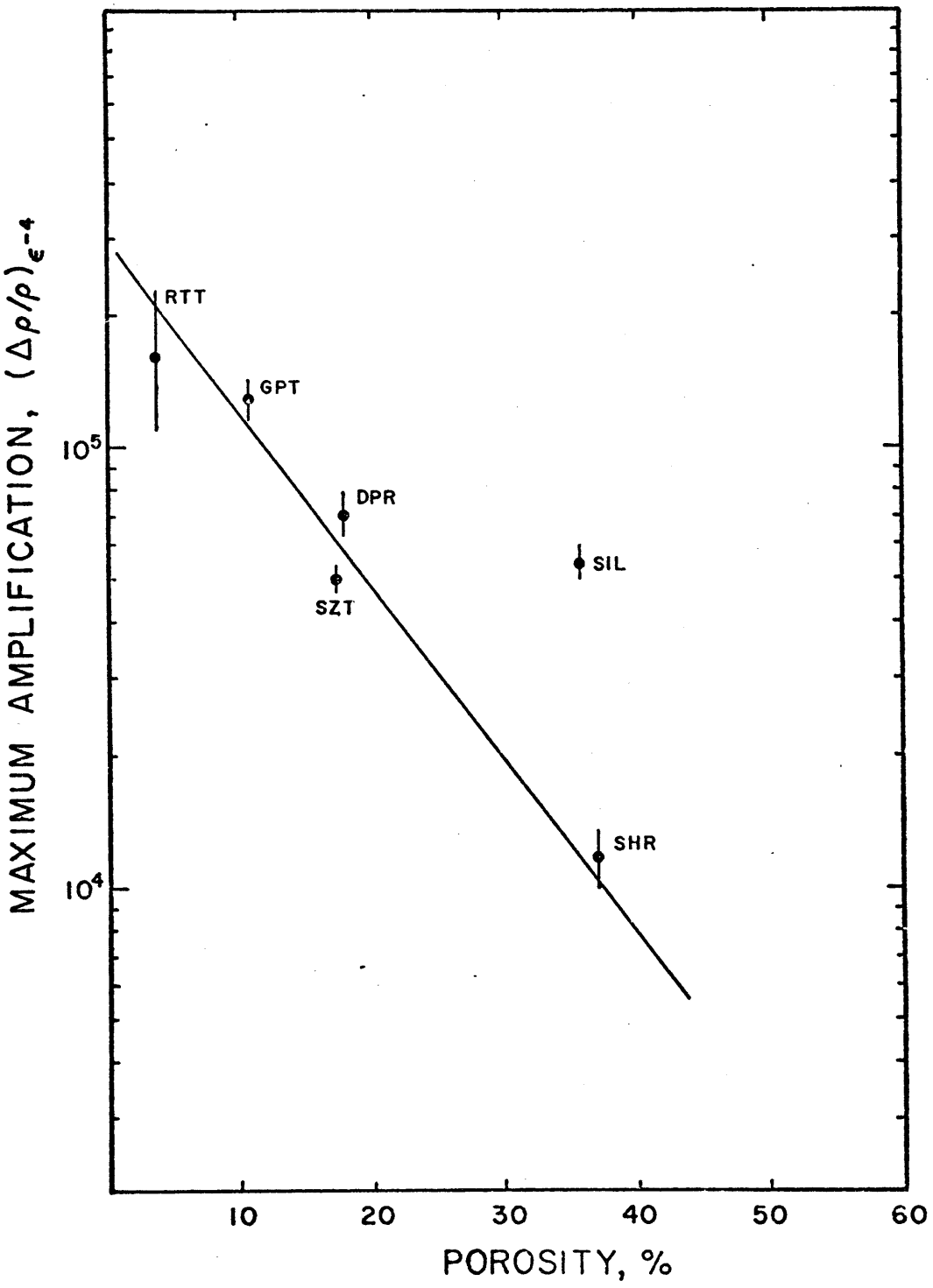

Figure 4.8 Maximum amplification of tuff samples vs. porosity

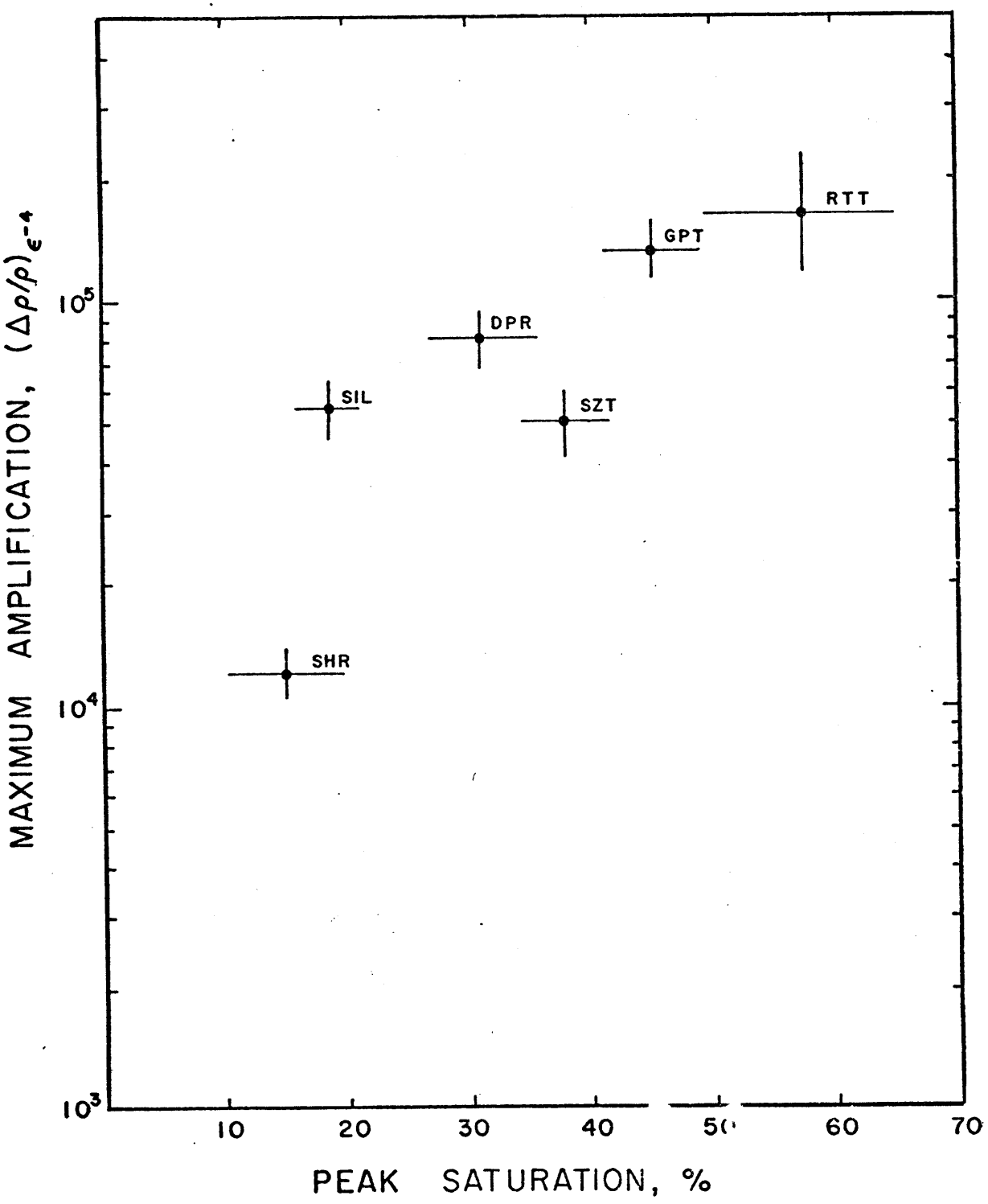

Figure 4.9 Maximum amplification of tuffs vs, peak saturation

Table 4.1 Strain Amplification of the California Tuffs

Sample	Saturation (%)	Amplification $(\Delta\rho/\rho)_{\varepsilon-4}$
GPT	100	2.9×10^{4}
	68	4.5×10^{4}
	45	1.3×10^{5}
	35	4.4×10^{4}
	17	3.3×10^{4}
	11	0
SIL	90	9.7×10^{2}
	53	1.0×10^{4}
	28	4.5×10^{4}
	18	5.5×10^{4}
	11	6.0×10^{3}
	8	8.8×10^{3}
	3	too dry
SZT	100	3.7×10^{3}
	89	6.5×10^{3}
	74	$\cdot.5\times10^{4}$
	38	5.0×10^{4}
	23	0

Sample	Saturation (%)	Amplification $(\Delta\rho/\rho)_{\varepsilon-4}$
RTTa	100	1.7×10^{5}
	83	4.2×10^{4}
	66	1.4×10^{5}
	47	2.3×10^{5}
	35	3.4×10^{4}
RTTb	82	5.0×10^{4}
	68	1.1×10^{5}
	53	2.4×10^{4}
DPRa	100	2.1×10^{3}
	75	1.5×10^{4}
	31	8.0×10^{4}
	11	6.4×10^{4}
	7	5.5×10^{4}
SHR	93	2.6×10^{2}
	72	1.1×10^{3}
	19	1.3×10^{4}
	14	5.9×10^{3}
	4	4.6×10^{3}

Table 4.2 Physical Properties of the California Tuffs

Sample	Porosity (%)	Modulus (GPa)	Peak Sat. (%)	Max. Amplification
GPT	10.7	10.0	45	1.3×10^5
RTT	3.7	12.5	58 (av)	2.3×10^5
DPR	17.9	3.5	31	8.0×10^4
SIL	35.6	2.4	18	5.5×10^4
SHR	37.2	2.2	14 (av)	1.3×10^4
SZT	17.1	3.3	38	5.0×10^4

CHAPTER V

Discussion

The electrical behavior of the rocks described above was similar to typical wet rocks studied elsewhere (Brace, Orange and Madden, [1965], Brace and Orange, [1968]), at least in certain respects. Conduction appears to be largely through water-filled pore space; surface conduction may be important, particularly for samples containing clays, but mineral conduction is probably not significant. An increase in stress lowers resistivity for partial saturation, as was the case for a granite (Brace and Orange, [1968]). However, there are at least two characteristics of the tuffs which are quite unusual, and require some discussion. First is the high amplification factor, and the second is electrical recoverability.

Amplification Factor

Madden has shown [1978] that amplification factor ranges from about 1600 (granodiorite of 0.4 percent porosity at 7.5 MPa) through 800 (granite of 0.9 percent porosity) to about 100 for porous sandstones. Amplification factor here was 10^3 to 10^5 (Figure 4.5) and 10^4 in Yamazaki's study.

Saturation and porosity seemed to be determining factors for electrical amplification of strains. Both high and low saturation tended to reduce amplification. At high saturation there is only a small percentage increase in the number of conduction paths before all the fluids have been mobilized. Amplification factors under these conditions would be low. As saturation decreases, a larger fraction of the water is initially in the form of isolated pockets that are subsequently joined. This situation leads to highest amplification. For still lower saturations, an increasing fraction of the water pockets do not join as stress is applied. The percentage of newly interconnected cracks is again low, and amplification is lower.

The stiffer rocks are not able to close cracks as well as the lower modulus samples for a given stress. It might be concluded that amplification would be low in this case. However, there are two factors that counter this argument. First, the higher water content in the stiffer rocks (at peak saturation) overcomes the fact that crack closure is not as effective. Second, the lesser pore volume tends to make small changes in interconnectivity more pronounced. This is particularly true for rocks with a greater fraction of cracks than pores. Less stiff rocks do not require as much water for maximum sensitivity because the crack closure

due to the larger strain is great enough to effectively distribute the water.

Yamazaki [1966] found that for rocks of about the same porosity, high amplification was associated with high permeability. Based on other studies, Brace, [1977], high permeability implies large pore diameter. Unfortunately, it was difficult to determine a meaningful pore diameter in all cases for these tuffs based on the SEM studies, so that his observation could not be fully tested here. The tentative conclusion was that amplification did not correlate with pore size. Clearly there is need here for further petrographic work.

Recoverability

In many ways the most puzzling behavior of the tuffs is the electrical recoverability during a stress cycle. No other partially saturated rocks show this effect to any degree. Two parameters seemed important: porosity and pore size. Porosity is the dominant factor; the most porous tuffs (35 percent) did not recover well. Recoverability improved as porosity decreased or equivalently, as modulus increased.

The more recoverable tuffs contained larger cracks and pores, and coarser mineral structures. In samples with pore diameters 100 times smaller (SIL), electrical resistance increased insignificantly upon unloading. Perhaps the fine gas bubble voids increased the capillarity within the sample, making it more difficult for water to retract as stress is decreased. Sandstones also showed consistantly poor electrical recoverability, probably a result of the difference in pore structures between the two rock types.

A third factor, and one which would be difficult to assess, must be surface properties of the different phases in the tuffs. Perhaps recoverability requires a nonwetting phase, such that water is dispelled from pores after stress is released. Unfortunately it was not possible to determine all the phases in the rocks, let alone their surface characteristics. This too is a fertile area for future studies.

CHAPTER VI

Conclusions

1) The rate of change of resistance with applied stress has been shown to be very large, particularly for small strains, in agreement with Yamazaki's results on certain tuffs from Japan.

2) Amplification factors as defined at a strain of 10^{-6} range between 10^3 and 10^5 for the California tuffs.

3) Porosity and saturation are the key factors for optimum amplification.

4) Tuffs exhibit an electrical recoverability not observed in other rock types.

5) Electrically sensitive tuffs exist near active faults where they could be used as stress monitors for earthquake prediction.

6) A preliminary investigation of electrical properties similar to the chunk test would seem appropriate for locating a field site, as a precise description of lithology for a suitable rock is not available at this time.

7) Further studies on mineralogy, pore structure and permeability would greatly improve the understanding of the processes involved.

APPENDIX A

Studies of Nevada and Montana Tuffs

The initial phase of this project was aimed at verifying the observations of Yamazaki and hopefully gaining some insight into the processes involved. Yamazaki demonstrated that the particular conditions of interest were low stress and low saturation. Therefore the approach chosen was to consider stresses only up to 6 MPa and saturation levels generally less than 25 percent.

Three samples from the Nevada Test Site and two from Montana were used in this first study (Table A1). The sample preparation and experimental procedure was exactly the same as discussed previously for the California tuffs. After testing these rocks, four sandstones were analyzed for a comparison of rock types (Table A1).

Observations

Stress-strain curves for the tuffs and the Pottsville and Berea sandstone are shown in Figure A1. Porosities are indicated next to the curves. These tuffs are more linearly elastic than many of the California rocks: there is little if any hysteresis in the curves. Sandstones usually retain a permanent strain after the stress cycle.

The effect of stress cycling on the electrical properties is apparent in Figure A2. Tunnel Beds tuff recoverd nearly completely upon successive loading, Berea sandstone did not. The second cycle of Berea showed almost no change in resistance. This behavior was typical of the other sandstones, as seen in Figure A3. Although the degree of recoverability varied among the tuffs, it was consistently poor in the sandstones.

If only the loading curves are considered, both the sandstones and the tuffs (with the exception of the Pottsville sandstone), have high amplification factors at low strains (Figures A4 and A5). Thus Yamazaki's unusual observations have been verified. The amplification factors as previously defined are compiled in Tables A2 and A3.

Discussion

Clearly rock type is an important parameter in the electrical characteristics of these samples. After the unrecoverable nature of the sandstones was observed, further studies were concentrated solely on tuffs.

There were no identifiable trends of amplification factor with porosity or saturation because the concept of "optimum saturation" discussed earlier had not yet been realized. The restricted range of low saturations led to some misleading initial conclusions. Low saturation was by forture ideal for Yamazaki's very porous rocks, but it is not a key factor when considering tuffs in general.

After the work on California rocks revealed the importance of saturation level, certain of the Montana and Nevada tuffs were re-tested at the saturations predicted from Figure 4.7. With little surprise, these rocks were consistent with the California samples and fell nicely on to the linear plot of Figure 4.7.

Table A1 Rock Descriptions

Sample	Location	Porosity (%)	Modulus (GPa)	Description
TBT	Nevada Test Site, Tunnel Beds area 20	17.6	4.1	Zeolitized ashfall tuff 20% phenocrysts: 5% quartz 15% plag & sanidine 5% lithic fragments 75% groundmass: 40% clinoptilolite 10% clay minerals 15% opal & silica minerals 10% glass
ATT	Ammonia Tanks tuff, Nevada Test Site, Silent Canyon Caldera	5.8	8.5	40% phenocrysts: 15% quartz 15% plag & sanidine 3% Ti rich augite 5% opaques 2% biotite 5% lithic fragments 55% groundmass: fine grained zeolitized ash & glass
RMT	Ranier Mesa tuff, Sleeping Butte Caldera segment, Nevada Test Site	14.2	8.5	phenocrysts: 10% quartz 10% plagioclase X% opaques X% Ti stained biotite 10% pumice fragments 70% fine grained groundmass: 10% zeolites 10% clay 50% ash
BLT	Butte, Montana	10.2	11.0	phenocrysts: 10% quartz 10% plagioclase 5% biotite 75% groundmass: 20% plag lathes X % chlorite 35% recrystallized glass 20% pumice fragments

Sample	Location	Porosity (%)	Modulus (GPa)	Description
FPT	Frying Pan Basin, Montana	29.6	4.6	5% phenocrysts: quartz 95% groundmass: pronounced vitroclastic texture; zeolites and clays radially lining glass shard structures, 20% disseminated opaques
Berea sandstone	Ohio, W. Virginia	17.2	6.5	orthoquartzite: 95% quartz & chert 5% feldspar
Mixed Co. (Kayenta)	source unknown	22.0	3	arkosic sandstone: 52% quartz 21% orthoclase 20% calcite 7% microcline opaque and lithic fragments
Navajo sandstone	source unknown	16.4	8.5	99% quartz 1% oxides
Pottsville sandstone	Spring city, Tenn.	3.0	7.5	46% quartz 41% orthoclase 11% muscovite 2% oxides

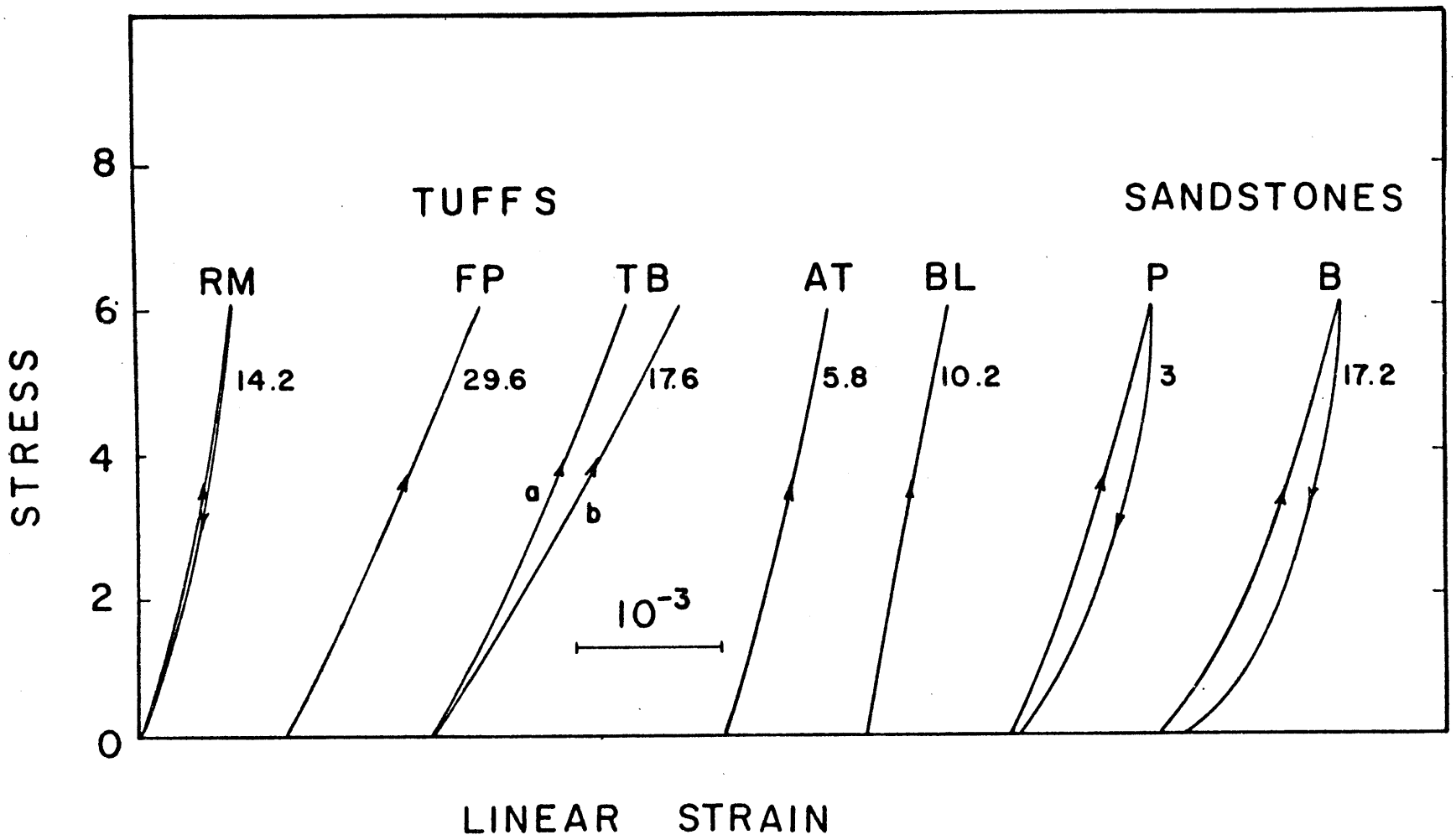

Figure A1 Stress-strain curves of Nevada/Montana tuffs and the Pottsville and Berea sandstones

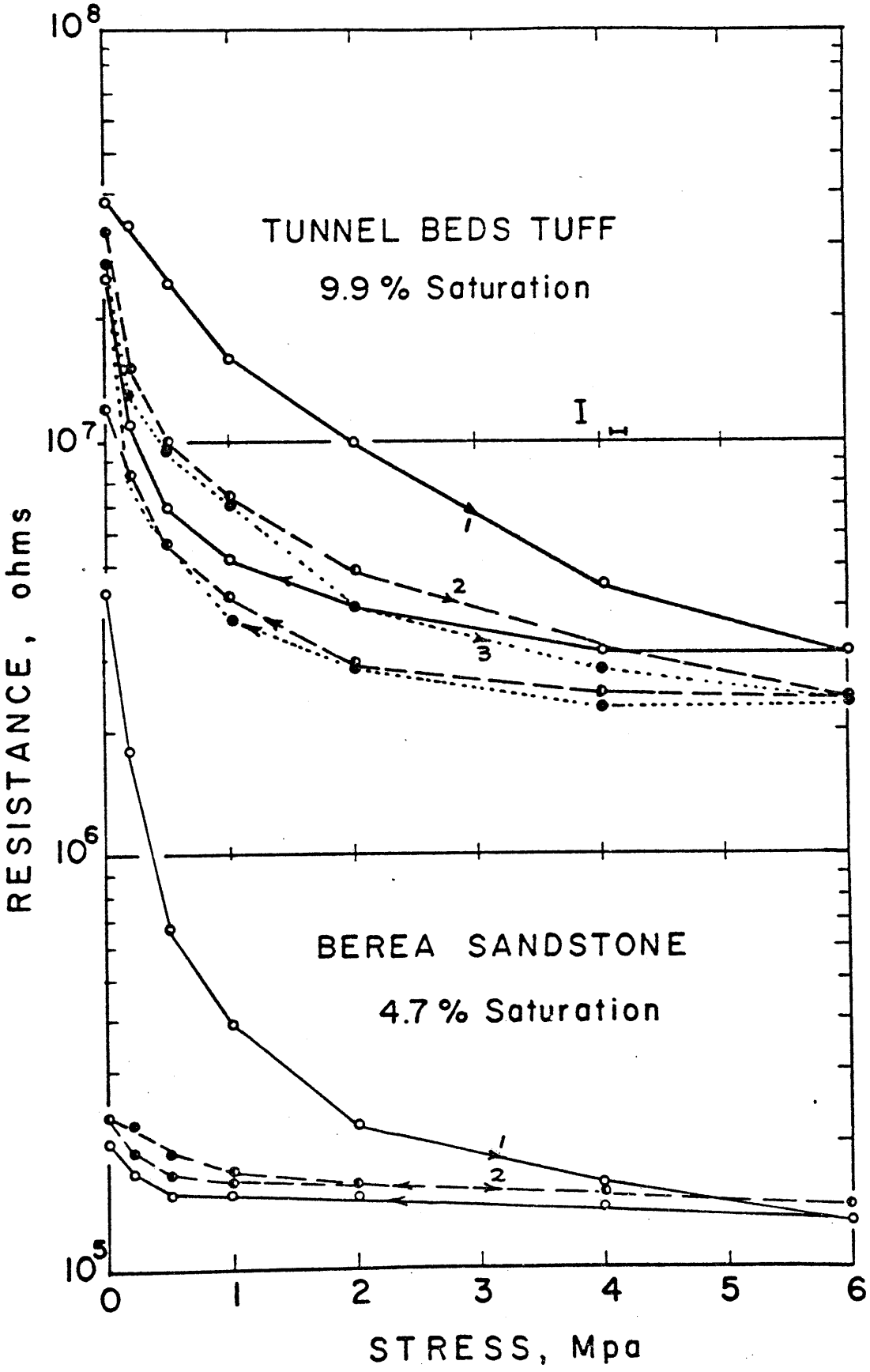

Figure A2 Change in resistance with stress, TBT, Berea ss.

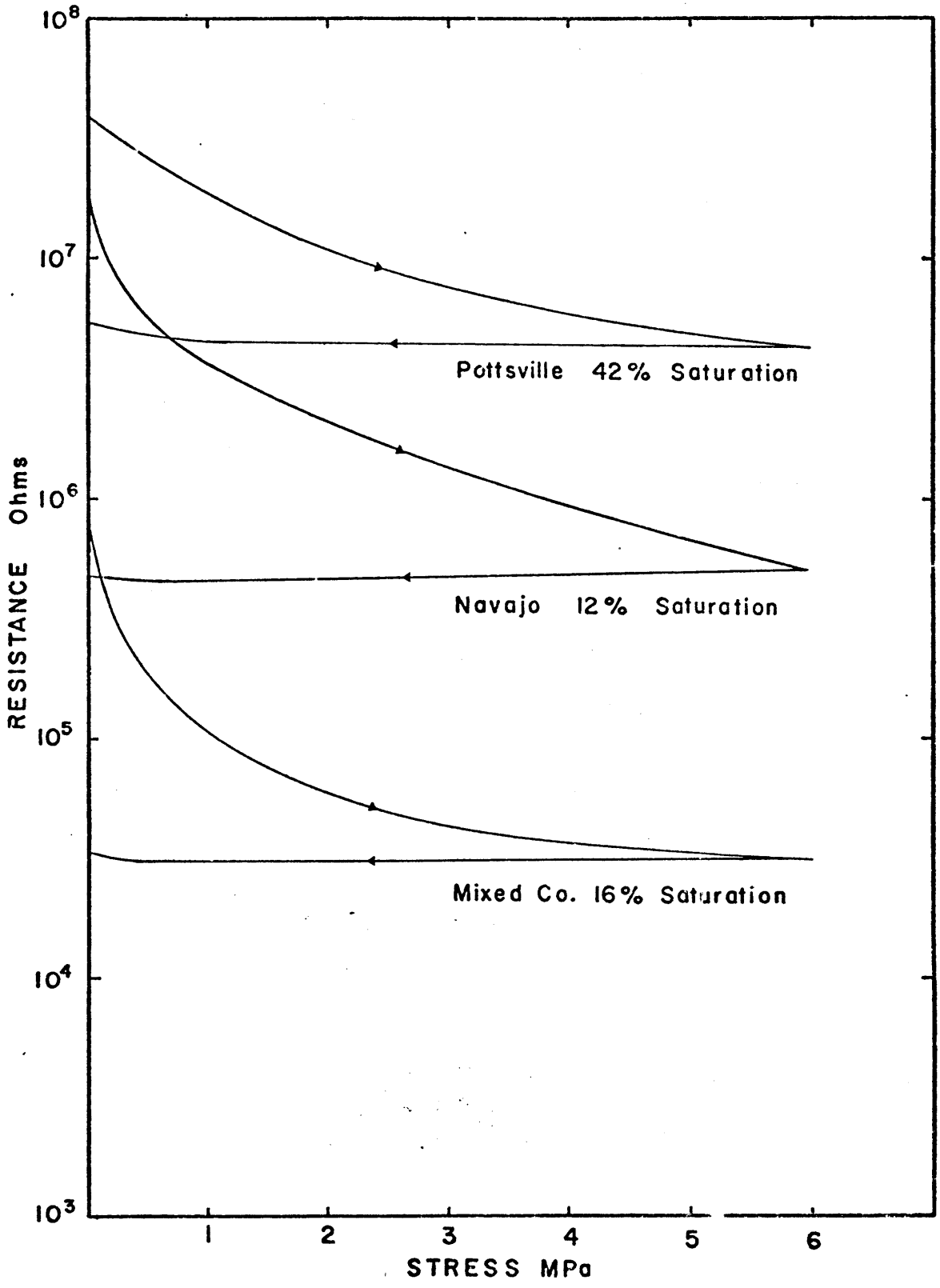

Figure A3 Change in resistance with stress: sandstones

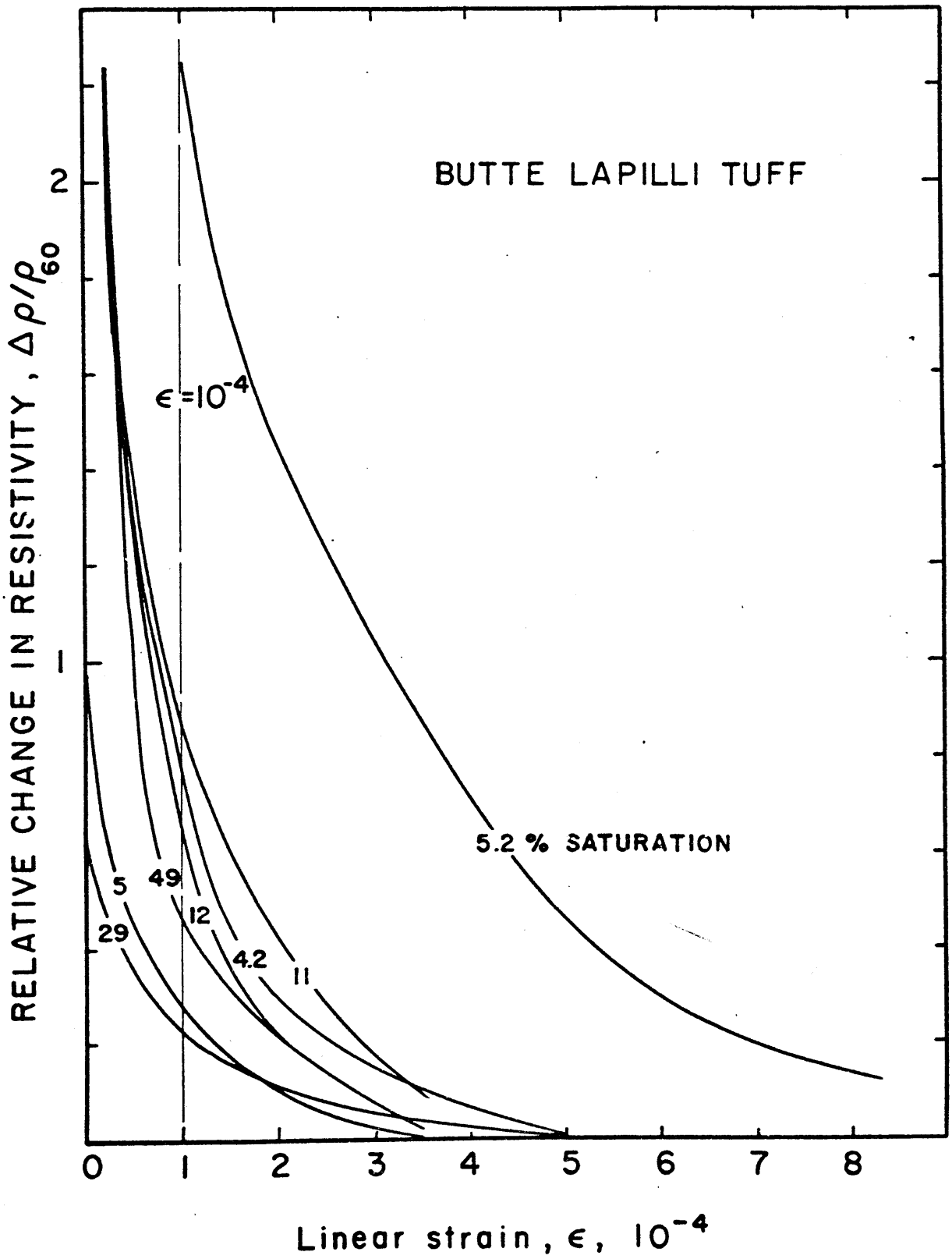

Figure A4 Relative change in resistivity with strain, BLT

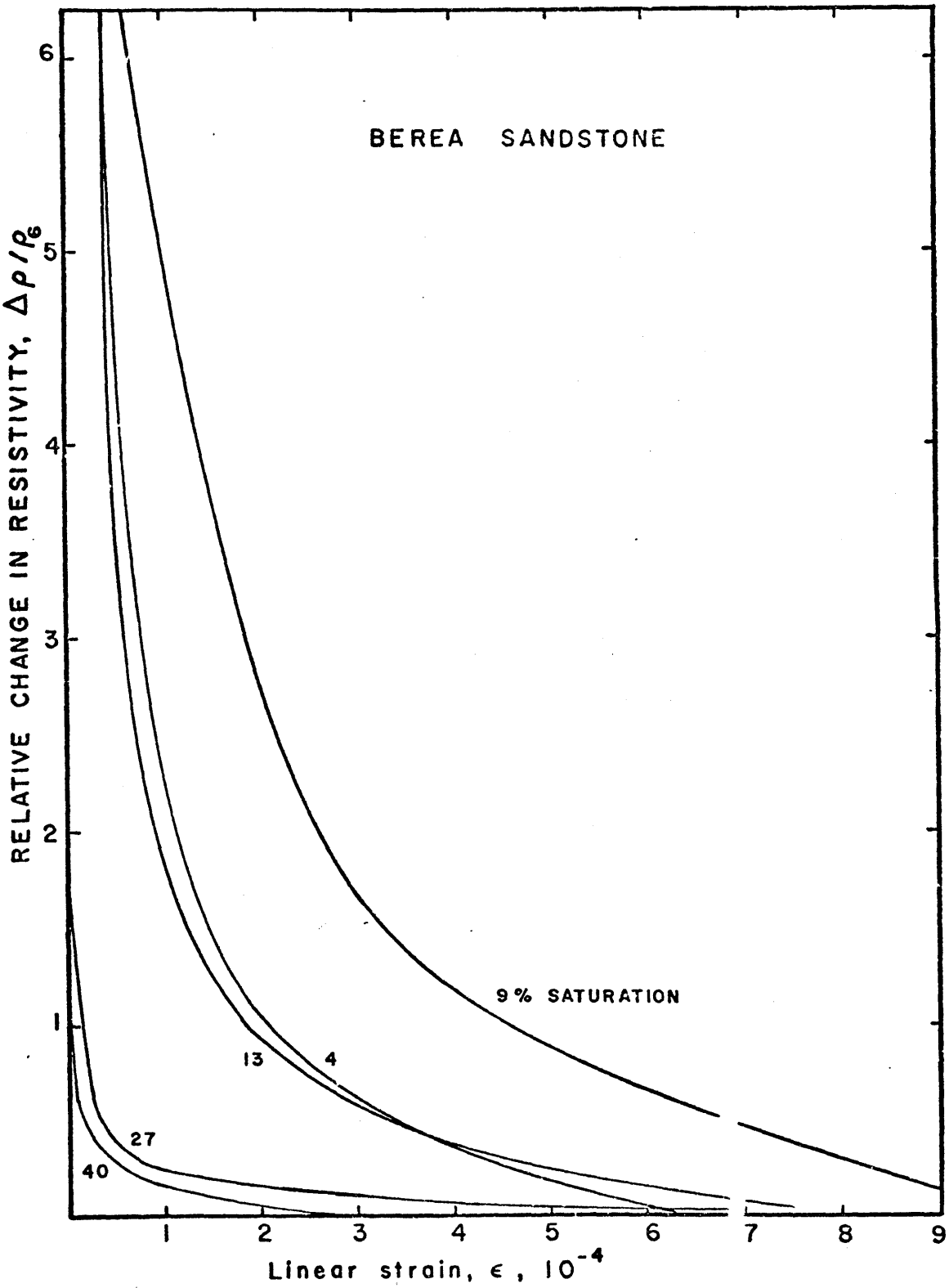

Figure A5 Relative change in resistivity with strain, Berea Sandstone

Table A2 Strain Amplification of the Montana/Nevada Tuffs

Sample	Saturation (%)	Amplification $(\Delta\rho/\rho)_{\varepsilon-4}$
BLT	4.2	2.3×10^{4}
	5.0	2.5×10^{3}
	5.2	1.6×10^{4}
	11.2	8.1×10^{3}
	12.6	2.1×10^{4}
	29.6	3.0×10^{3}
	49.1	2.8×10^{4}
RMT	2.5	5.0×10^{2}
	4.7	0
	5.1	5.0×10^{2}
	5.4	6.6×10^{2}
	38.0	1.0×10^{4}
	45.0	1.6×10^{4}
TBT	2.8	7.0×10^{3}
	4.8	8.0×10^{3}
	7.3	8.0×10^{3}
	9.9	1.0×10^{4}
	12.9	1.0×10^{4}
	20.1	4.4×10^{3}
	46.8	2.0×10^{3}

Sample	Saturation (%)	Amplification $(\Delta\rho/\rho)_{\varepsilon-4}$
FPT	2.1	2.2×10^{3}
	3.8	1.2×10^{3}
	6.7	1.7×10^{3}
	15.2	3.2×10^{4}
	17.1	2.4×10^{3}
	22.2	8.8×10^{4}
	58.0	8.0×10^{2}
ATT	7.0	1.2×10^{2}
	11.1	1.3×10^{2}
	14.3	1.5×10^{3}
	18.6	5.0×10^{2}
	56.0	1.0×10^{4}

Table A3 Strain Amplification of Sandstones

Sample	Saturation (%)	Amplification $(\Delta\rho/\rho)_{\varepsilon-4}$
Mixed Company (Kayenta)	3.8	9.2×10^{2}
	7.6	4.0×10^{2}
	21.8	1.0×10^{4}
	34.3	1.6×10^{3}
	44.0	0
	94.0	0
Navajo	2.5	3.1×10^{3}
	5.6	2.4×10^{4}
	12.3	3.2×10^{4}
	19.3	9.2×10^{3}
	33.0	8.6×10^{2}
Berea	4.7	4.4×10^{4}
	9.2	3.9×10^{4}
	13.1	1.2×10^{4}
	26.9	1.6×10^{3}
	40.0	9.1×10^{2}

Sample	Saturation (%)	Amplification $(\Delta\rho/\rho)_{\varepsilon^{-4}}$
Pottsville	6.4	0
	8.5	0
	13.9	0
	21.0	0
	24.9	0
	32.5	0
	42.5	1.3×10^{0}
	63.4	1.0×10^{-1}

APPENDIX B

The Chunk Test

This test was devised to quickly investigate the electrical properties of samples while still in a crude hand specimen configuration. Results were strictly qualitative, as the geometry factors of the irregular shapes were not precisely known. However, chunk tests performed on the Nevada and Montana tuffs showed that resistance cycled in the same manner as the cylindrical samples described in Appendix A, although to a lesser degree due to the larger sample size. Therefore, the chunk test was indeed valid for a preliminary sorting by electrical properties. Table B1 lists the samples used in this test along with their locations, and a brief hand specimen description.

Sample Configuration

Rock fragments were broken off into more or less equal shapes about 5 cm long. Two lead sheets, 0.02 cm thick by 1.9 cm square were conformed on to opposite sides of the sample, with copper wire soldered to each sheet, leading to the resistance measuring circuit. The lead was epoxied around the edges to the rock to avoid separation. The whole assemblage was then potted in Dow Corning Sylgard 186

silicone elastomer with the wires extending out of the cylindrical case of rubber (Figure B1).

Experimental Procedure

Potted samples were placed in a beaker of kerosene or water inside a 15 cm diameter argon gas pressure vessel. Kerosene is prefered to prevent corrosion of the vessel. However, Sylgard swells in kerosene and the samples must then be coated with Kenyon K-Kote to avoid expansion, a process which adds a few days to the sample preparation.

Resistances were measured at natural water content by method 2 of Appendix D, while increasing and decreasing hydrostatic pressure to a maximum of 5 MPa. The set-up is schematically illustrated in Figure B2.

Data

Figures B3 through B5 show the electrical resistance response to stress cycling on a number of the California tuffs. Samples which exhibited little or no change are not included. The unloading curves consistently fell below the loading curves as with the cored rocks.

Samples are ordered in terms of relative resistance change in Table B2. Those with an asterisk were the ones chosen for more detailed study. Some very sensitive rocks were not selected because of their friability.

Table B1 Location and Hand Specimen Descriptions of the California Tuffs

Sample	Location	Hand Specimen Description
PIN	Pinnacles National Monument	Dense green tuff, numerous lithic fragments and phenocrysts
SJB	San Juan Grade Rd. (Salinas Rd.), San Juan Bautista	Conglomerate in tuffaceous matrix, pebbles up to 0.75 cm in diameter
COT	Stony Point Quarry, Cotati	Fine grained powdery grey clay in 0.5 cm thick bed
CMV	Coomsville Rd., Napa	Plum colored matrix, lithic fragments up to 1 cm, plagioclase lathes visible
MWT	Montecello Rd., Napa	Welded grey pumice fragments, light and porous
SIL	Silverado Trail, St. Helena	White rhyolitic tuff, fragments of white pumice up to 1 cm, lithic fragments (0.5 cm), plagioclase lathes
PET	Petrified Forest Rd., Calistoga	Rhyolitic tuff similar to Silverado, more weathered & friable
SHR	St. Helena Rd., St. Helena	Coarse, grey, hard and very crystalline tuff, extensive and well exposed in road cuts
DPR	Deer Park Rd., Sunset Point	Very dense fine grained purple and grey matrix with large pores; no noticeable lithic fragments

Sample	Location	Hand Specimen Description
RLS	Robert Louis Stevenson State Park, Calistoga	Very hard grey tuff weathers to yellow-brown; lithic fragments up to 0.5 cm; fractured
GPT	Little Grizzly Peak, Berkeley Hills	Large massive outcrop, coarse and dense lithic fragments up to 2 cm, highly fractured
RTT	Round Top Hill, Berkeley Hills	Basalt tuff; black, fractured and weathered into boulders; part of a cinder cone 400 m in diameter
SZT	Siesta cinder cone Siesta Valley	Brown lithic tuff filled with veins of zeolite
DRY	Grizzly Peak Rd., Berkeley Hills	Buff colored airfall tuff, weathered and friable layer a few meters thick

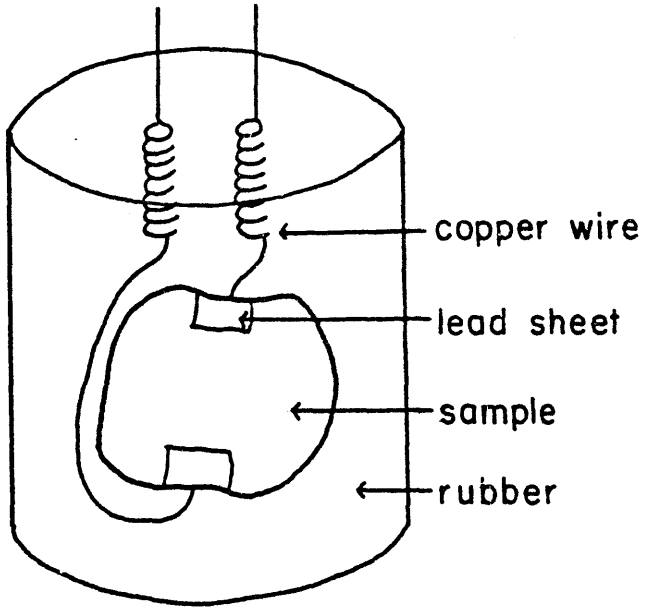

Figure B1 Sample configuration for the chunk test

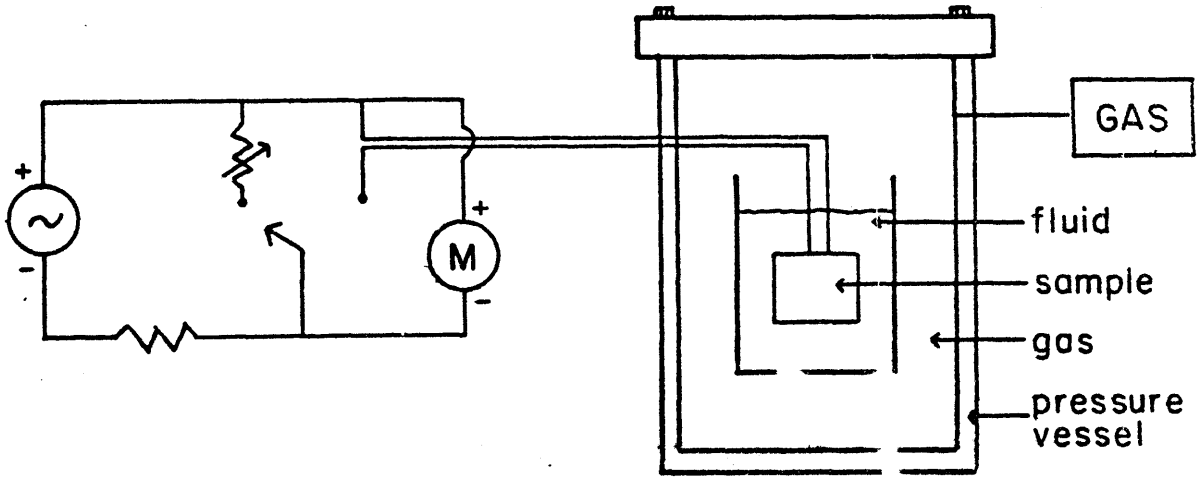

Figure B2 Chunk test experimental apparatus

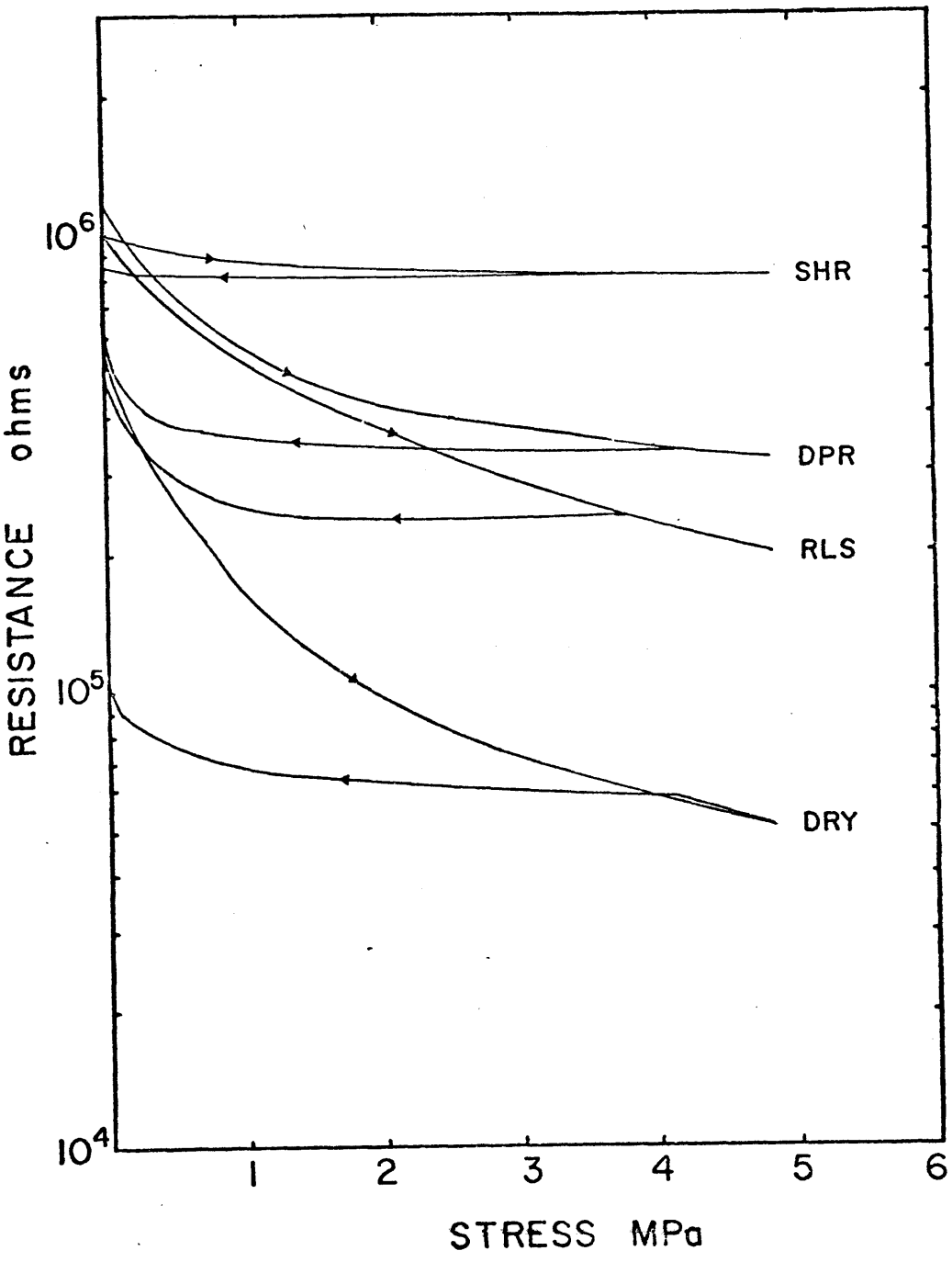

Figure B3 Change in resistance with stress; SHR, DPR, RLS, DRY.

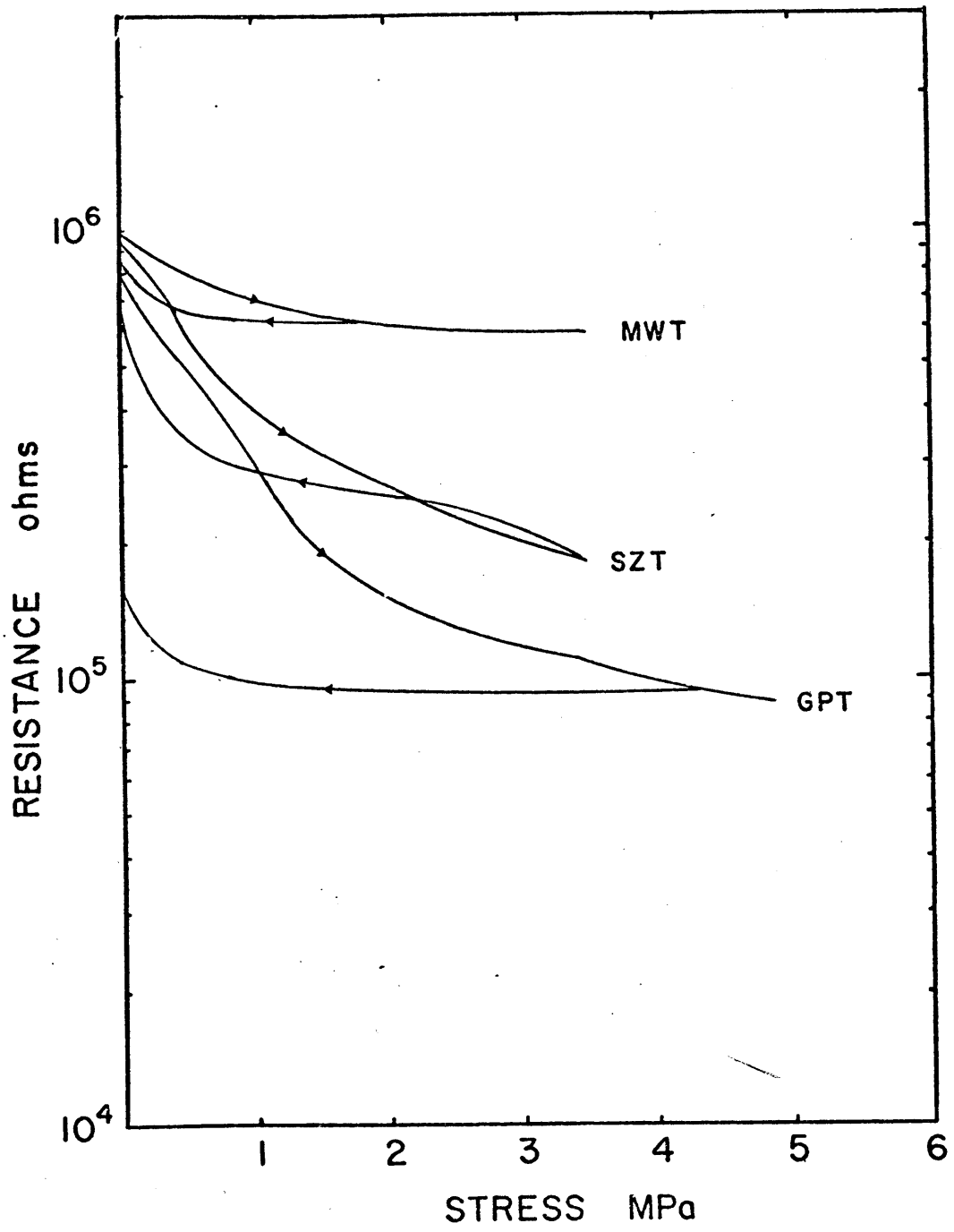

Figure B4 Change in resistance with stress; MWT, SZT, GPT.

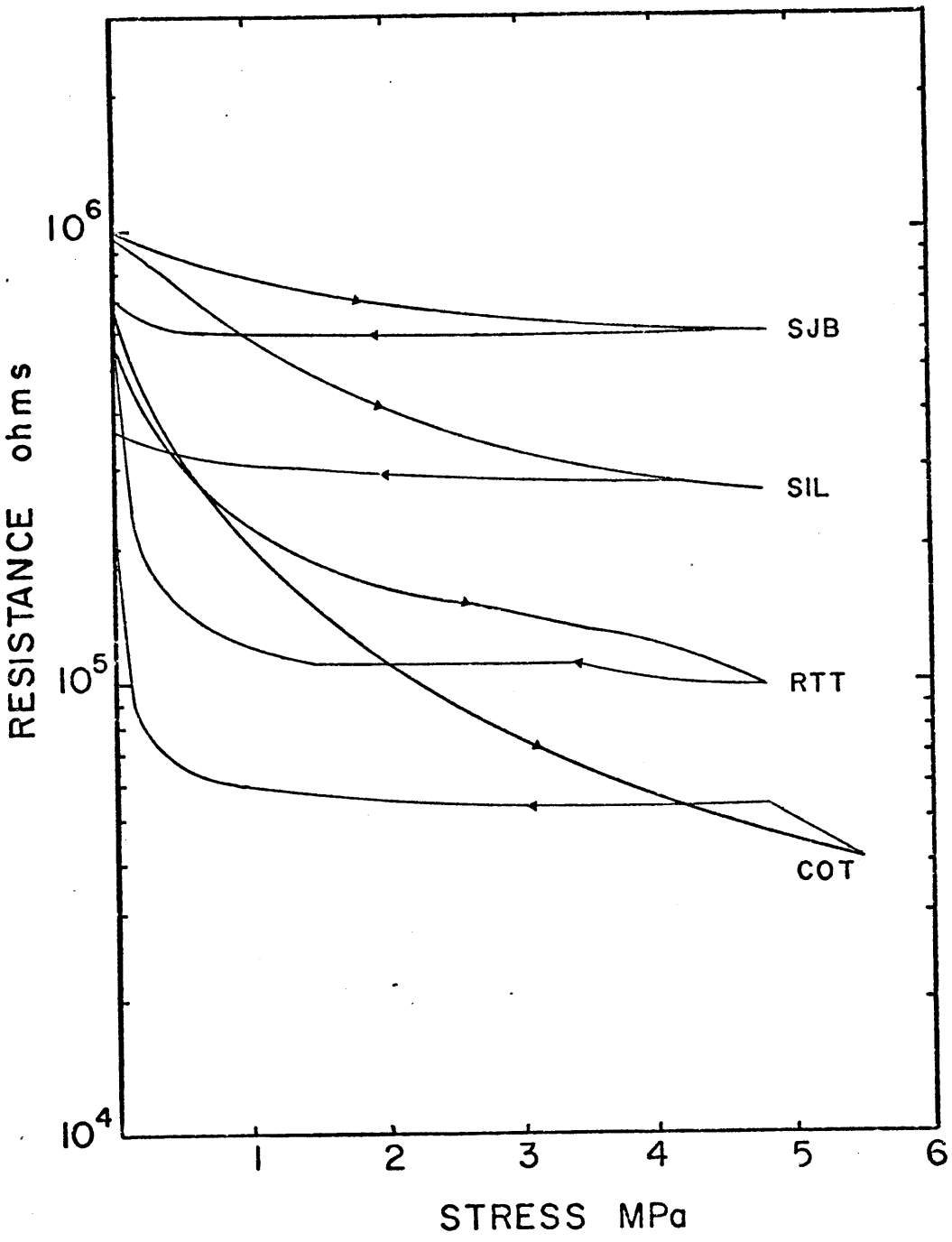

Figure B5 Change in resistance with stress; SJB, SIL, RTT, COT.

Table B2 Relative Ordering of Electrical Properties of California Tuffs

Good	Fair	Poor	No Effect
COT	SZT*	SHR*	CMV
DRY	RLS	SJB	PET
GPT*	DPR*	MWT	PIN
RTT*	SIL*		

* Studied in detail

APPENDIX C

Stress-Strain and Electrical Behavior of Selected California Tuffs

This section contains the complete set of data on the California tuffs that were not included in chapter 4, as they are similar to the examples shown there. Stress-strain curves for the six tuffs are illustrated in Figure C1. Figures C2 and C3 show the change in resistance with stress for each sample at an arbitrary saturation. The curves were chosen to show the most typical electrical recoverability of that sample. Figures C4 through C8 are plots of the relative change in resistivity with strain and were derived from the stress-strain and resistance data.

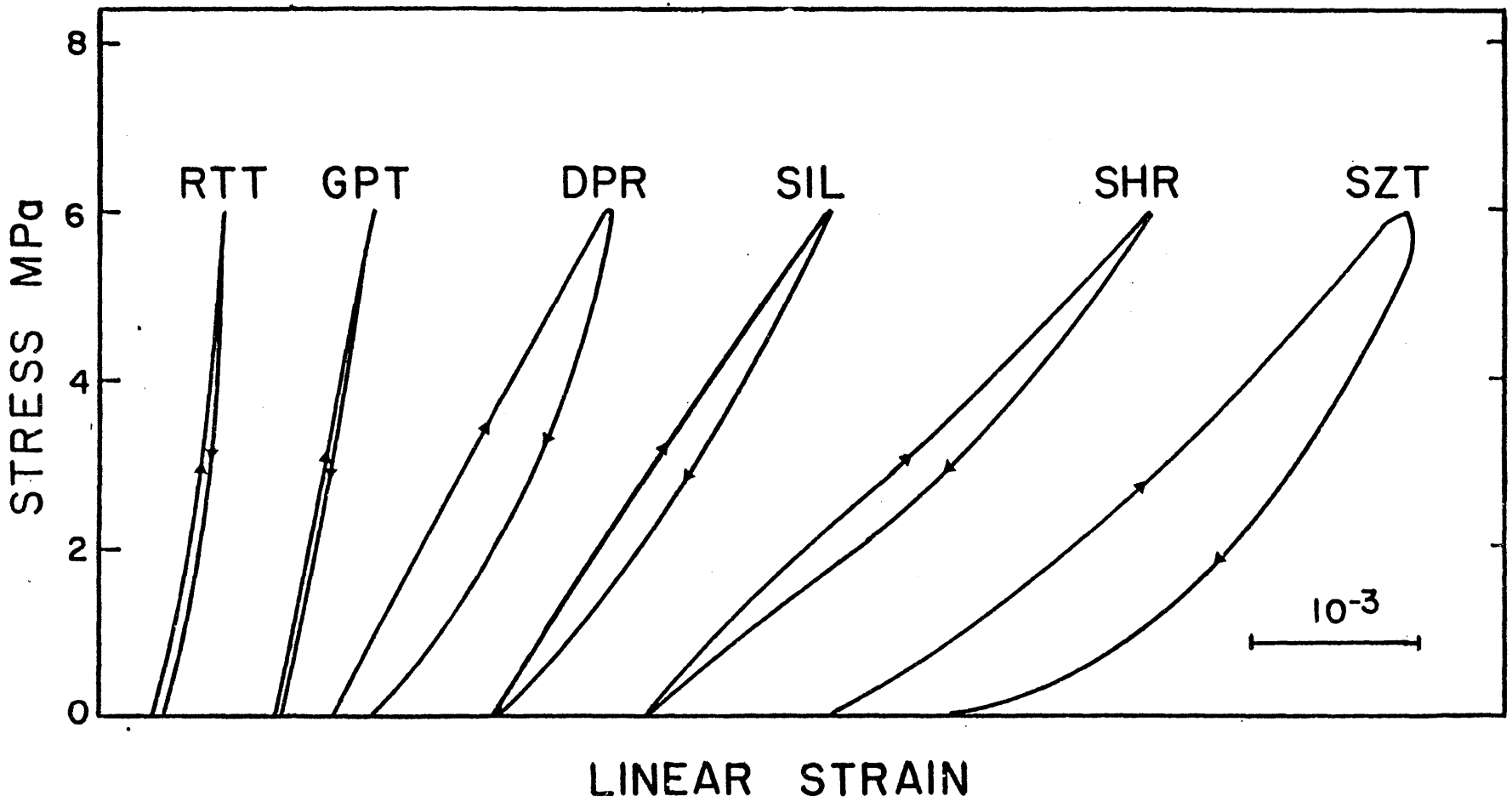

Figure C1 Stress-strain relation for the California tuffs

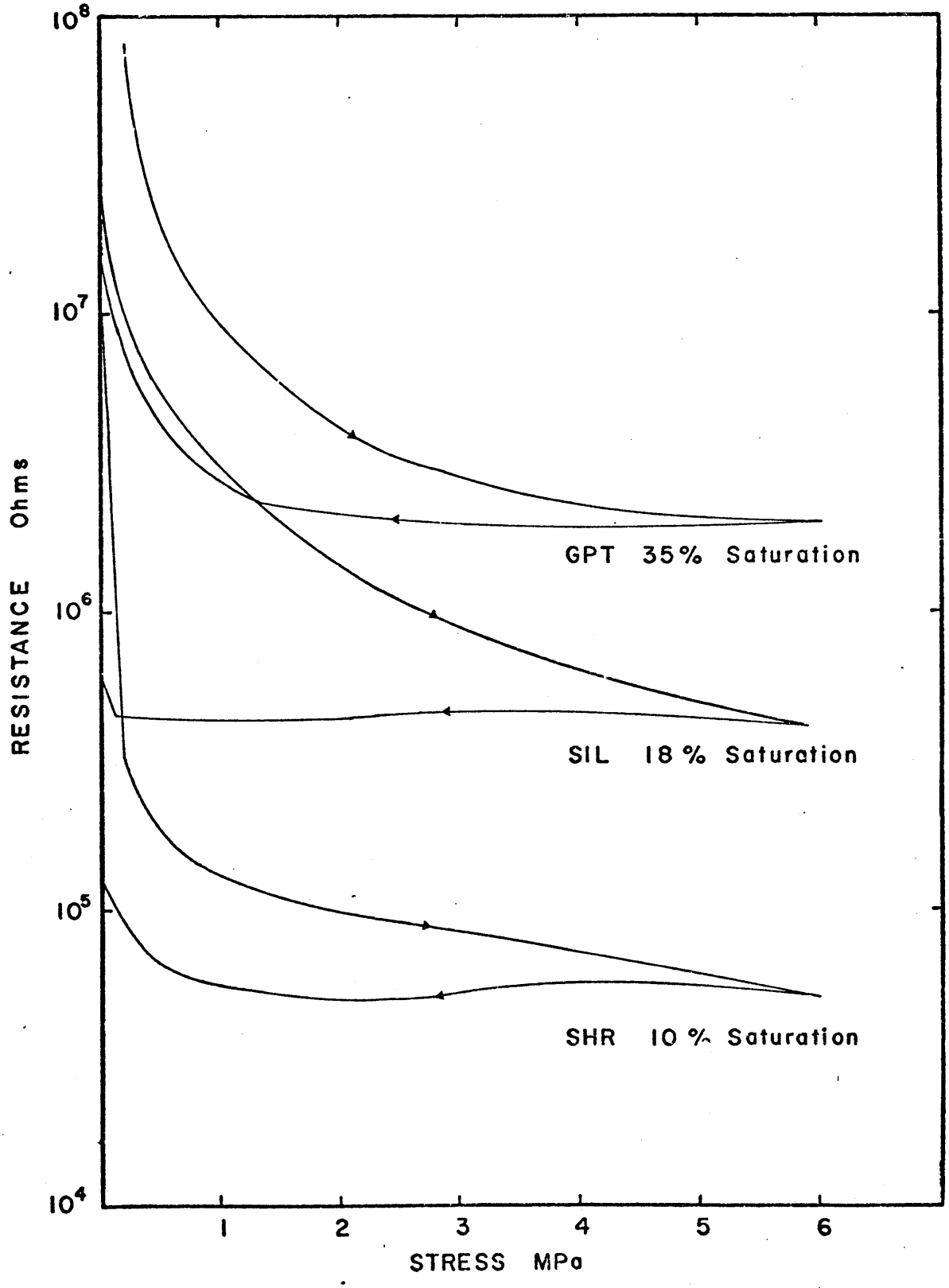

Figure C2 Change in resistance with stress; GPT, SIL, SHR.

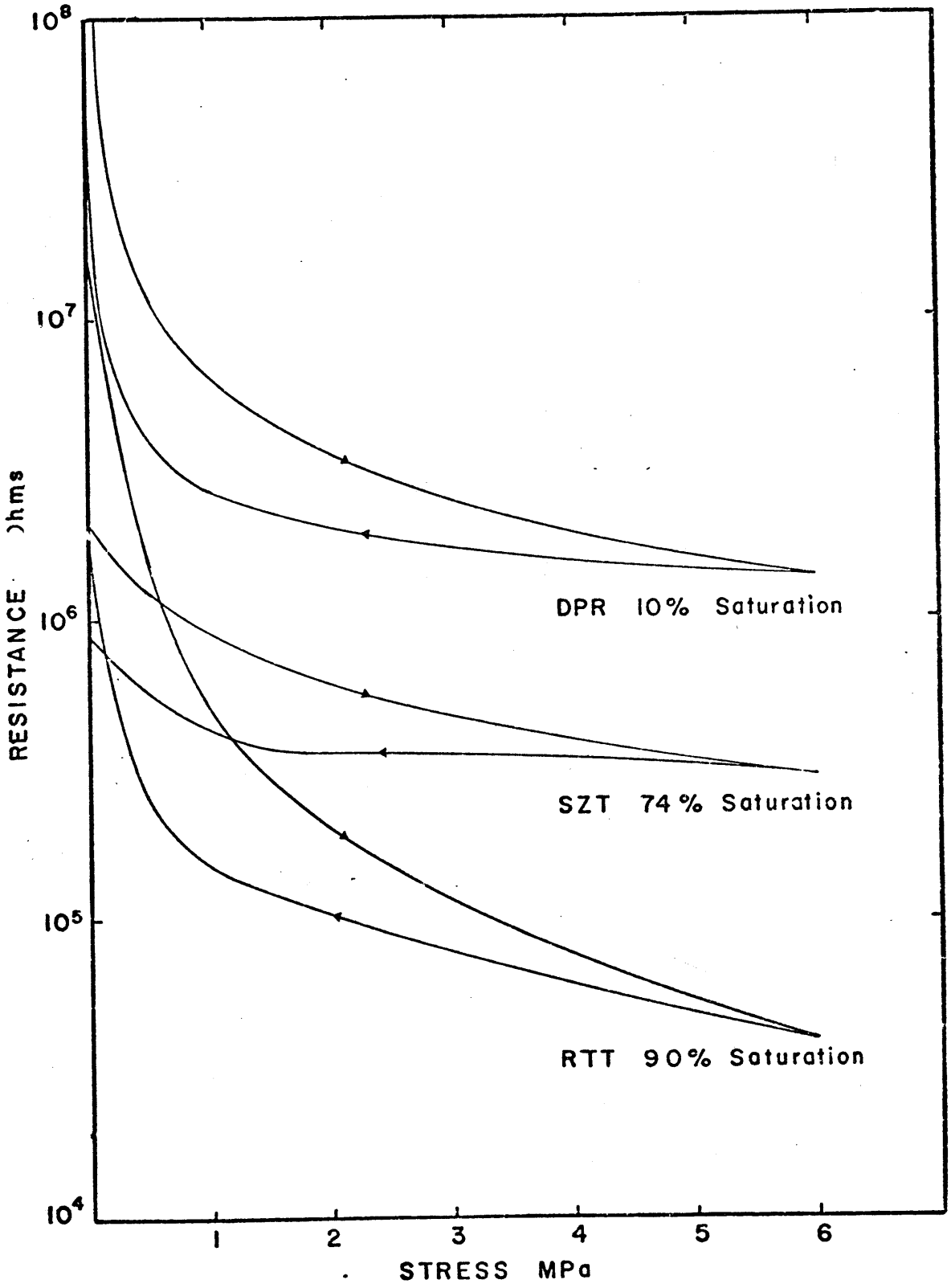

Figure C3 Change in resistance with stress;
DPR, SZT, RTT

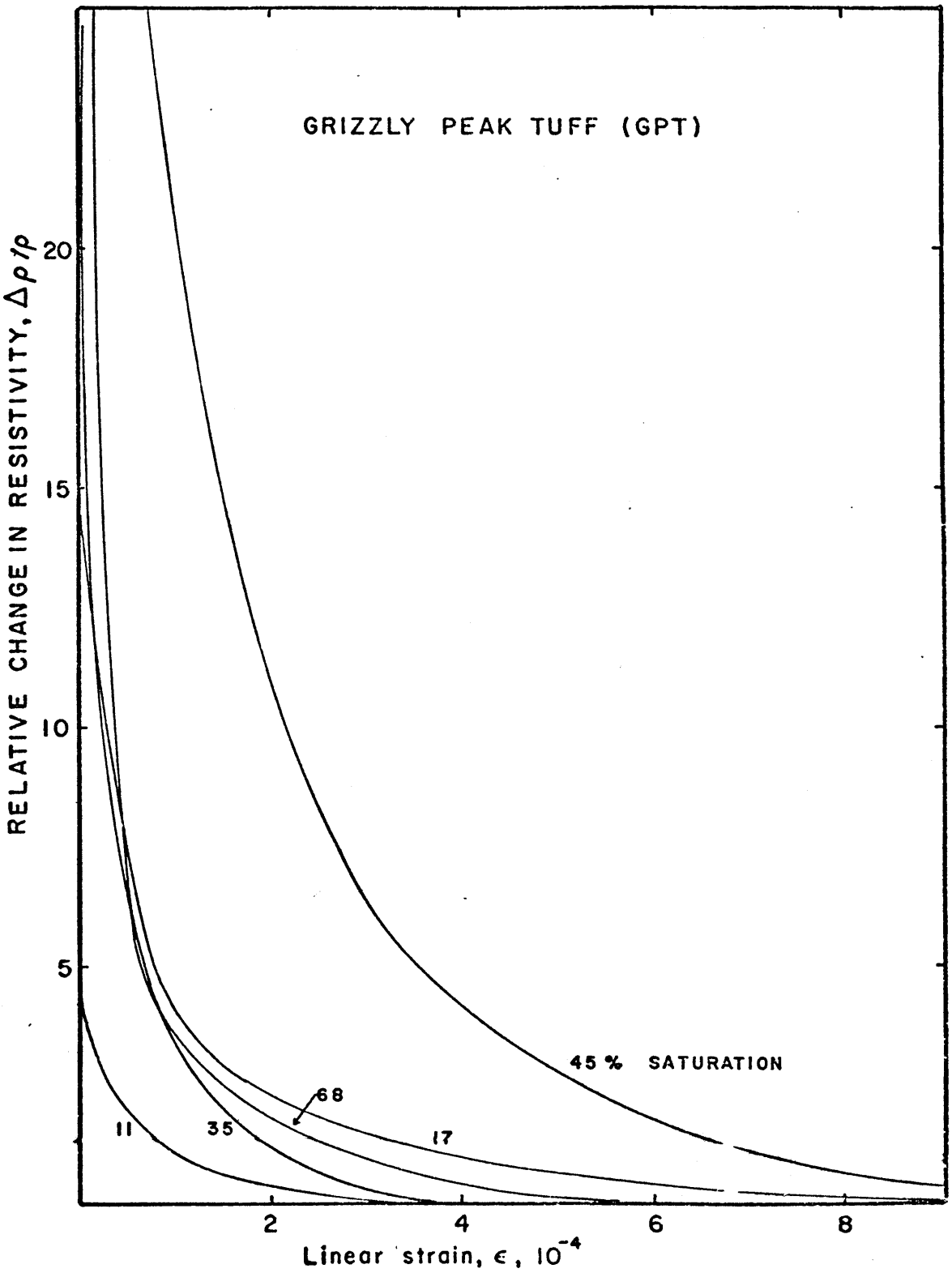

Figure C4 Relative change in resistivity with strain, GPT

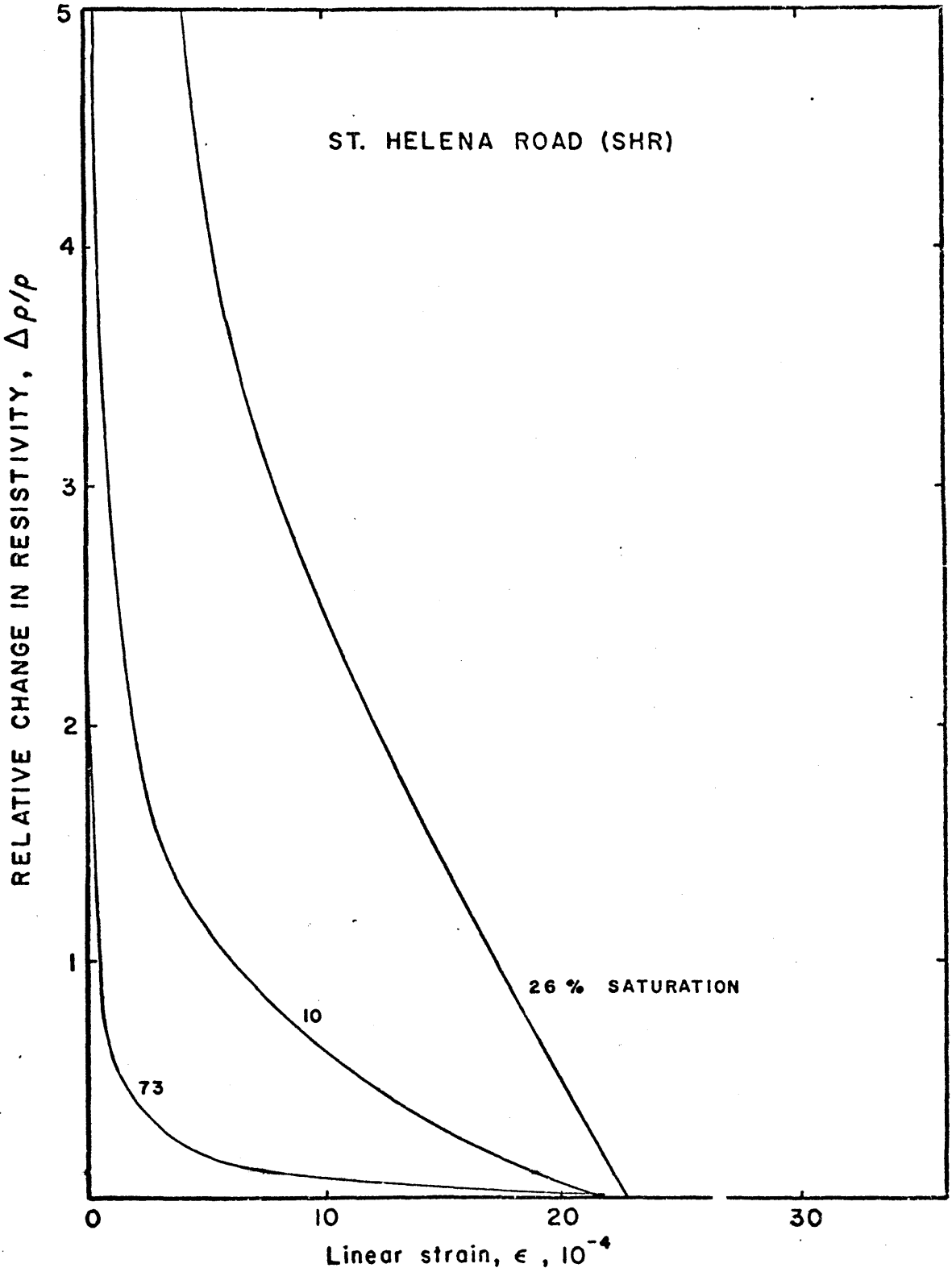

Figure C5 Relative change in resistivity with strain, SHR

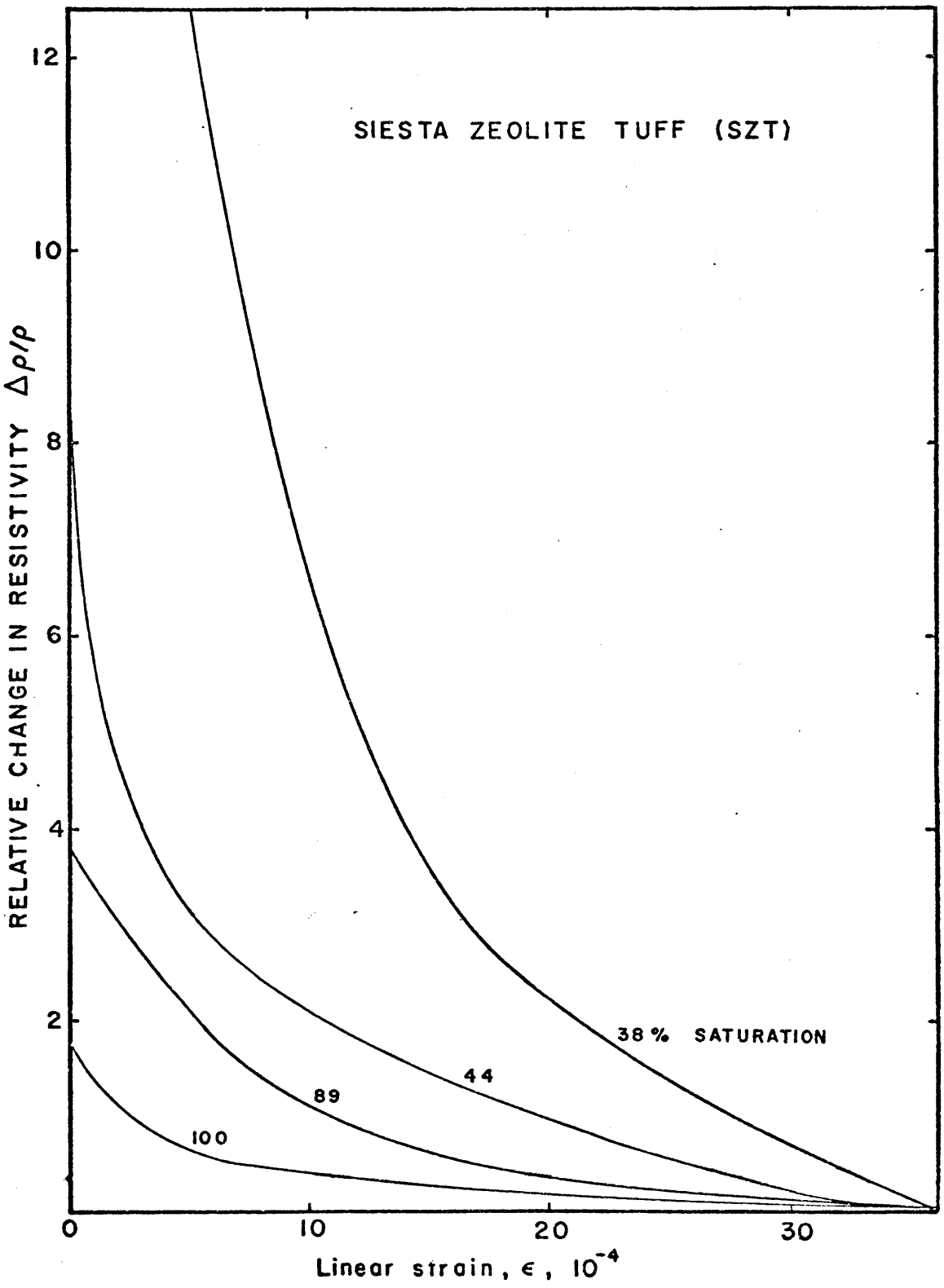

Figure C6 Relative change in resistivity with strain, SZT

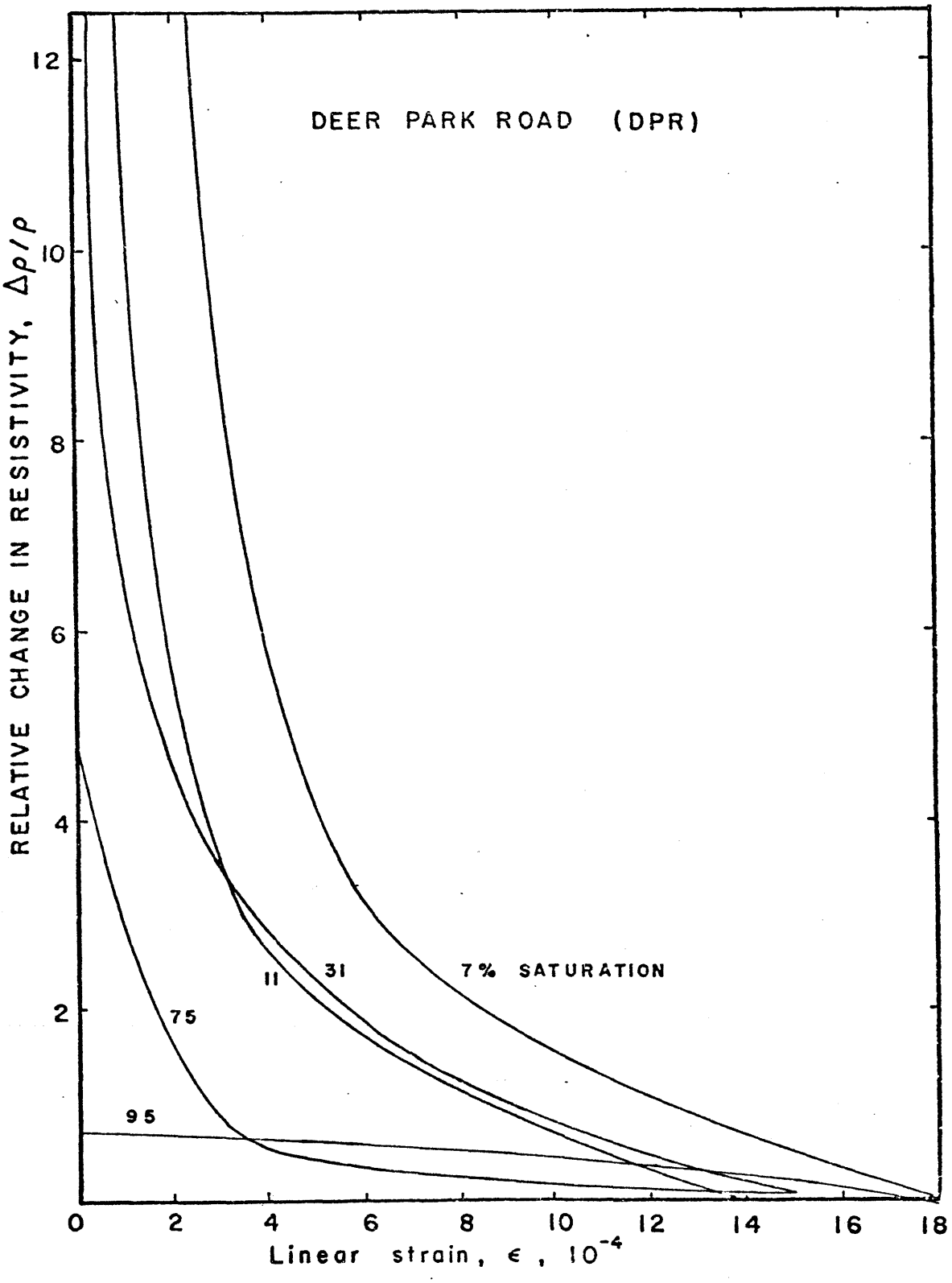

Figure C7 Relative change in resistivity with strain, DPR

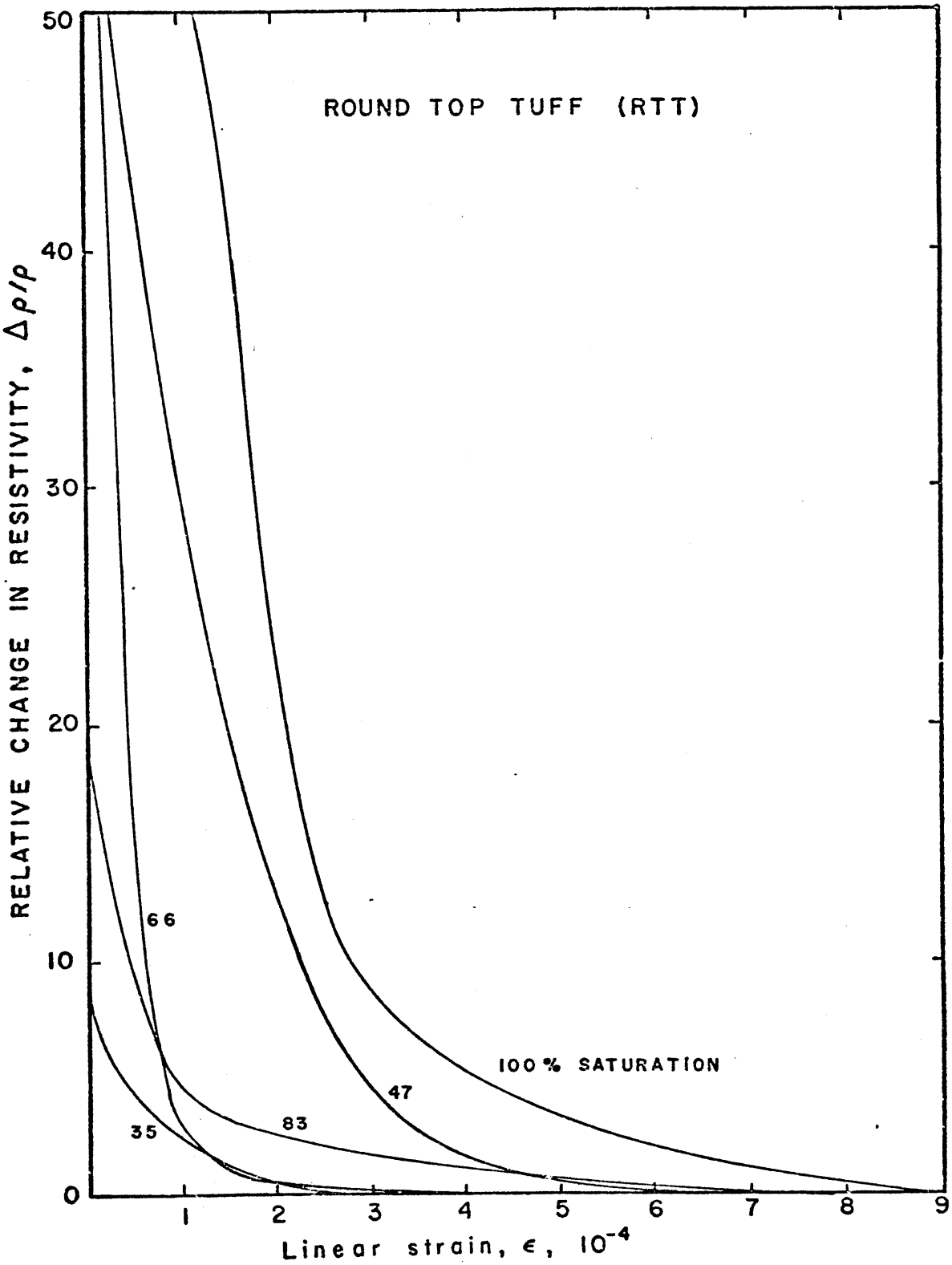

Figure C8 Relative change in resistivity with strain, RTT

APPENDIX D1

Resistance Measuring Techniques

There are several techniques for measuring the resistance of a rock, each with trade-offs on ease and accuracy. Most of these methods involve matching the voltage across a variable resistance decade with that across the rock sample. In all cases, the source voltage was kept at 10 Hz AC, to minimize any frequency effects that could occur at higher frequencies. See Appendix D2 for a more complete description of frequency effects.

Method 1.

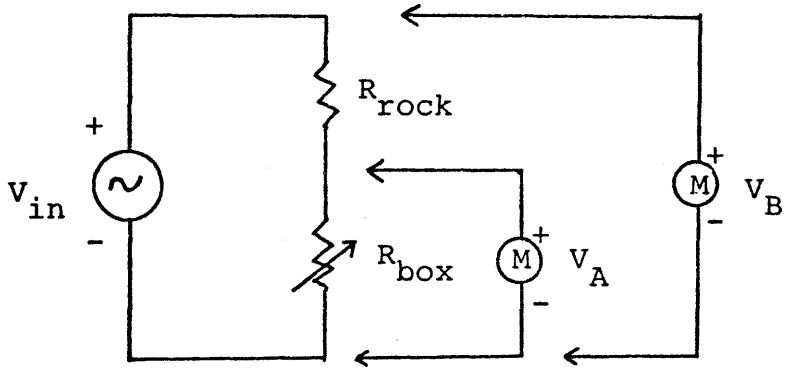

The particular circuit used for the early work on the Nevada and Montana tuffs was the same as that in Brace, Orange and Madden, [1965]. V_A and V_B are measured on a vacuum tube volt meter (HP model 400H). From the above circuit diagram, it follows that $V_{in}=V_B$ and the system is a voltage divider where

$$\frac{V_A}{V_{in}} = \frac{R_{box}}{R_{rock} + R_{box}}$$

Since R_{box} is known and a particular V_A/V_{in} is chosen, then R_{rock} can be calculated. To simplify the calculation, assume that R_{box} is much less than R_{rock}, by appropriately adjusting the voltage ratio.

$$\text{Now} \quad R_{rock} = R_{box} \left(\frac{V_{in}}{V_A}\right)$$

The ratio V_A/V_{in} is determined to make the resistance fall in a reasonable range on the decade box and to introduce no significant errors. For example, with $V_{in}/V_A = 100$, $R_{rock} = 100R_{box}$. (Turn the voltmeter range down by two orders of magnitude to measure V_A, then adjust the decade until the meter needle comes to the same point as it did for V_B).

A 1% theoretical error is introduced because $R_{exact\ rock} = 99R_{box}$. The difference is considered negligable. By turning the voltage down in this manner, it is possible to measure rock resistances that are greater than the resolution of the variable resistance decade.

The advantage of this technique is that it is quick and requires no calculation. In order to find the resistance of the rock, one need only add two orders of magnitude on to the resistance read off the decade box. Most of the Nevada and Montana tuff samples were measured in this way.

Problems: Since the signal to be measured on the meter has been reduced substantially, there is a potential problem of noise dominant errors. In fact if $V_A/V_{in} = 1000$, the signal to noise ratio is high enough that the measured resistance of the rock will have a noticeably large error (as much as a factor of 10). In the noise dominant situation, if V_A/V_{in} is chosen to be 1/10 instead of 1/100 or 1/1000, then the signals are larger and the resistance box gives better resolution. The exact formula for R_{rock} must be used, otherwise there is a 10% error: $R_{rock}=9R_{box}$.

On the practical side, this choice of V_A/V_{in} is not as quick, as it requires more mental gymnastics to calculate 9R than 10R. However, it is more accurate.

If the resistance of the decade, which has a maximum of 1 megohm, approaches the input impedance of the meter, then the effective resistance is reduced:

$$\frac{1}{R_{effective}} = \frac{1}{R_{box}} + \frac{1}{R_{meter}}$$

$$R_{effective} = \frac{R_{box} \cdot R_{meter}}{R_{box} + R_{meter}}$$

The effective value is substituted into the R values:

$$\frac{V_A}{V_{in}} = \frac{R_{box}}{R_{rock} + R_{box}} \quad \text{becomes} \quad \frac{V_A}{V_{in}} = \frac{R_{effective}}{R_{rock} + R_{effective}}$$

The HP 400H voltmeter has an input impedance of roughly 2.5 megohms. This impedance is rather low and should be taken into account when dealing with dry rocks whose resistance can be as high as 10 megohms.

Method 2.

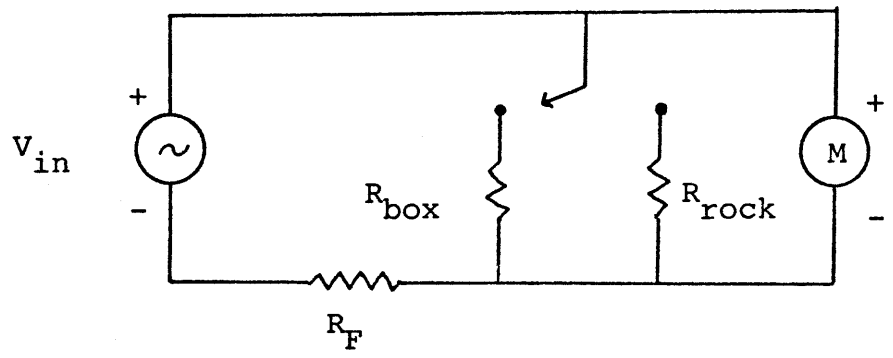

Method 2. involves the same technique of matching voltages as method 1. A voltage is chosen with the switch on R_{rock}. Then with the switch on R_{box}, the resistance is adjusted until the same voltage is obtained as through the rock. Now $R_{rock}=R_{box}$. An additional resistor R_F is necessary in this circuit otherwise V_{meter} always equals V_{in}.

Choice of R_F: To find a suitable value of R_F, the sensitivity of the meter is analyzed with respect to the power transfer between the circuit and the load (rock). By Joule's Law,

$$P = I^2 R_F = \left(\frac{V}{R_F + R_r} \right) R_r = \frac{V^2 / R_r}{(1 + R_F / R_r)^2}$$

According to this equation, the power in the load is zero if the resistance of the rock is either very small, or very large. Thus there must be some optimum value where the power is a maximum. Differentiate and equate to zero:

$$\frac{dP_{rock}}{dR_{rock}} = \frac{V^2}{R_{rock}} \frac{2R_F/R_r^2}{(1 + R_F/R_r)^3} + \frac{V^2}{(1 + R_F/R_r)^2} \frac{-1}{R_F^2} = 0$$

$$\frac{2R_F}{R_{rock}} = 1 + \frac{R_F}{R_{rock}}$$

$$R_F = R_{rock}$$

Therefore, a value of R_F should be chosen that is close to the expected value of R_{rock} for maximum sensitivity of the meter (greater accuracy in matching voltages). This method was used in the "chunk tests" on the California tuffs mainly because it is fast, and a switching box (R =1 megohm) was readily available courtecy of D. Johnston.

A problem arises when R_{rock} is greater than the maximum R_{box}, mainly low saturation rocks. If the voltage range of the meter is switched down as in method 1, the same simplifying assumptions can not be made.

$$V_{in}\left(\frac{R_{rock}}{R_{rock} + R_F}\right) = V_{M1}$$

$$V_{in}\left(\frac{R_{box}}{R_{box} + R_F}\right) = V_{M2}$$

If $V_{M1} = 100V_{M2}$, then

$$\frac{R_{rock}}{R_{rock} + R_F} = 100\ \frac{R_{box}}{R_{box} + R_F}$$

$$R_{rock}R_{box} + R_{rock}R_F = 100R_{box}R_{rock} + 100\ R_{box}R_F$$

$$R_{rock}(R_F - 99R_{box}) = 100\ R_{box}R_F$$

$$R_{rock} = \frac{100R_{box}R_F}{R_F - 99R_{box}}$$

Since $R_F = 10^6$ ohms,

then $$\boxed{R_{rock} = \frac{10^8 R_{box}}{10^6 - 99R_{box}}}$$

This is true if R_{meter} is much greater than R_{rock}. Otherwise the same problem with a low impedance meter exists because the meter is in parallel with the rock and the box.

$$\frac{1}{R_{\text{box effective}}} = \frac{1}{R_{\text{box}}} + \frac{1}{R_{\text{meter}}}$$

$$\frac{1}{R_{\text{rock effective}}} = \frac{1}{R_{\text{rock equation in box}}} - \frac{1}{R_{\text{meter}}}$$

As can be seen from the above discussion, the switching box method is no longer quick when trying to measaure high impedance rocks.

Method 3.

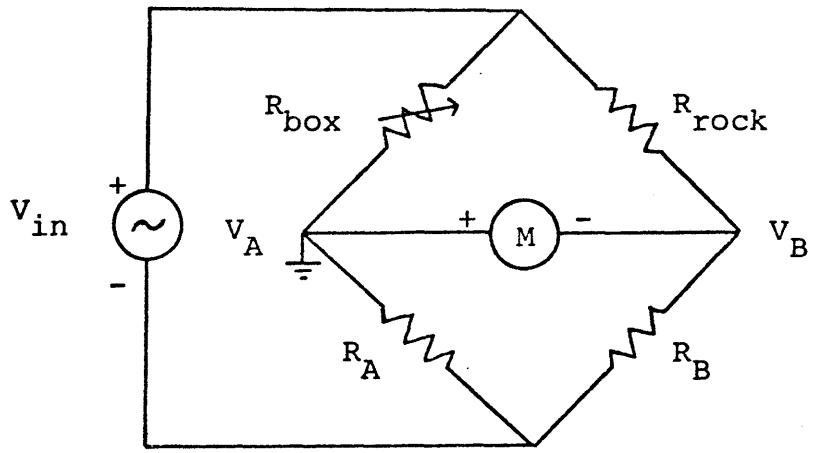

Bridge method: R_A and R_B are fixed resistors. R_{box} is adjusted until the bridge is balanced, i.e. the meter reads zero volts. Then $V_A = V_B$.

$$\frac{V_A}{V_{in}} = \frac{R_A}{R_A + R_{box}} = \frac{R_B}{R_B + R_{rock}} = \frac{V_B}{V_{in}}$$

$$R_A(R_B + R_{rock}) = R_B(R_A + R_{box})$$

$$R_{rock} = \frac{R_B}{R_A} R_{box}$$

Note that the response does not in any way depend on the meter. The ratio of R_B to R_A is chosen to scale R_{box} to R_{rock}. For instance, if $R_{rock\ max}$ = 10 megohm and $R_{box\ max}$ = 1 megohm, then make R_B/R_A=10. Now resistance measurements greater than R_{box} can be made. The absolute magnitudes of R_B and R_A are set to gain the maximum meter sensitivity to the null. R_B is chosen to be around the same order of magnitude as R_{rock}. (See sensitivity derivation in method 2). Then $R_A \simeq$ 100 kilohm for a typical low saturation rock. This value is optimum for the decade box, since it has maximum resolution in the middle ranges.

Because the resistance of the rock can vary widely depending on the mineralogy and degree of saturation, say between 1 kilohm and 10 megohm, it may be best to have two sets of resistors for optimum sensitivity. Each set has appropriate values of R_A. This modification is not tremendously important to the workings of the circuit unless there is reason to be concerned with sensitivity.

$$R_B = 10 \text{ kilohm for } 1 \text{ kilohm} < R_{rock} < 100 \text{ kilohm}$$

$$\text{and } R_B = 1 \text{ megohm for } 100 \text{ kilohm} < R_{rock} < 1 \text{ megohm}$$

The bridge method has a definite advantage over the other two methods. Since the meter does not enter into any calculations, there are no errors due to low input impedance or noise.

A problem common to all techniques: The source for the resistance measuring circuit has an alternating current of 10 Hz. The strain gauge and corresponding circuit on the other hand runs on DC, and is designed to detect small changes in the DC voltage. Since the AC and DC currents are juxtaposed in the sample, there is a coupling in which the AC current appears in the strain signal. The epoxy between the rock and strain gauge is not always enough to ensure proper insulation, particularly with saturated samples. The result is a 10 Hz vibration of the pen along the strain axis as much as 2 cm wide, (leading to a mighty fuzzy stress-strain curve!).

There are two solutions:

1) Disengage the pen while making a resistance measurement. This tends to slow down the experiment, since there are thirteen measurements to be made on each run, therefore twenty-six times to flick the pen. The chance for human error arises since one sometimes forgets to engage the pen after a measurement, and part of the stress-strain curve is lost.

2) Build a low pass filter into the chart input. A somewhat detailed description of the filter is in order as it has a significant effect on the chart response.

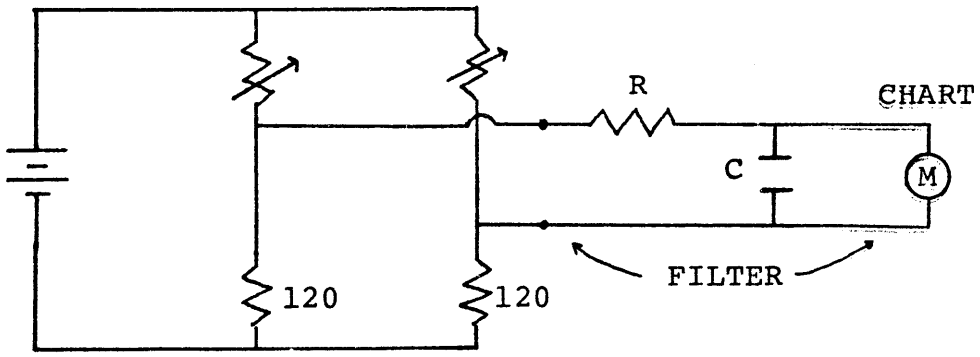

A standard low pass filter has response

$$\frac{V_{out}(s)}{V_{in}(s)} = \frac{1}{1 + sRC}$$

s= complex frequency $2\pi f$
R= resistance
C= capacitance

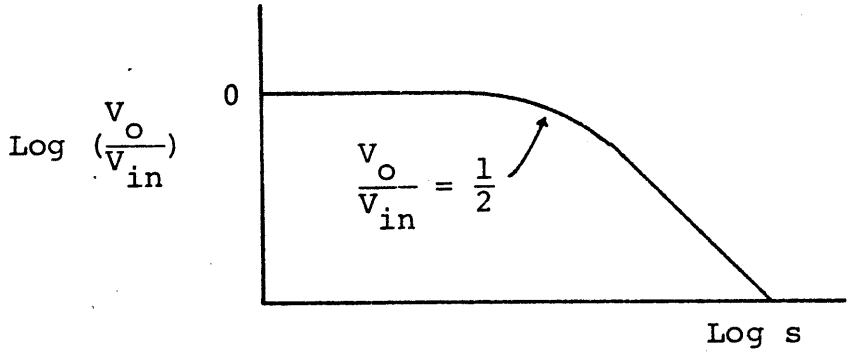

Above some cutoff s=1/RC, the response drops by 20 db/decade. (i.e. V_o/V_{in} goes as 1/s). Since it is not advantageous to vary s, for reasons stated in Appendix D3, R and C are chosen such that 10 Hz is well above the cutoff. On the other hand, if the cutoff is too low, the pen will respond sluggishly since the filter causes a time delayed response which goes as $e^{-t/\tau}$.

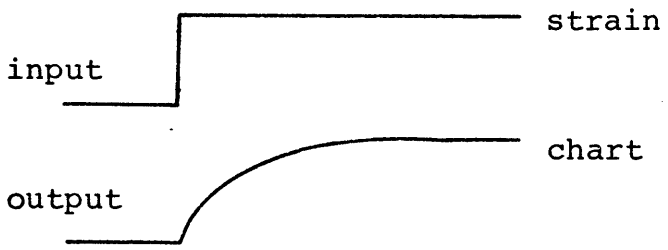

Thus if the strain is changed quickly (say instantaneously), the pen will not quite catch up to the true value of strain and the stress-strain curve will be slightly incorrect. This is a real problem because 10 Hz is quite a low frequency. There are tight constraints imposed on T_{max}, where 10 Hz is just at the break point of the response curve, and T_{min}, a value that will not cause noticeable delay in the pen.

The solution is to make sure that the stress is not pumped up or released too fast, to allow time for the delayed response. This introduces the question of strain rate dependance of the system as a whole. The point of the experiment is not to include strain rate as a parameter. However, running a relatively slow test for response reasons goes hand in hand with the fact that there must be time allowed for the rock to equilibrate to the new stresses. The pore water must redistribute, a factor dependant on permeability.

Note that if the experiment were run at a higher frequency, then "sluggishness" could be avoided altogether. When the amplitude of the noise is low, a smaller capacitor can be used to alleviate the response problem. At even higher frequencies, say 10 kHz, the pen will not even have time to respond to the noise.

Both solutions to the noise problem have their disadvantages. One might wonder why the resistance is not measured with DC. This would require the actual movement of ions through the sample. If it is assumed that the charge is being transmitted primarily by the water phase rather than by mineral conduction, then a DC current would tend to electrolyze the water. At one of the electrodes there would be dissociated water forming oxygen and hydrogen gas. This is far from a desirable situation, especially since fixed partial saturation is an important factor in the experiment.

APPENDIX D2

Choice of Electrode Material

The ideal electrode material for measuring resistance should have the following qualities:

1) Be a good conductor.
2) Maintain a good electrical contact with the sample
3) Have no stress effect (change in measured resistance with applied stress).
4) Have no frequency effect, or at least no frequency effect within a given working range.

Four different electrode combinations were tested with a 20 kilohm resistor in the following configuration:

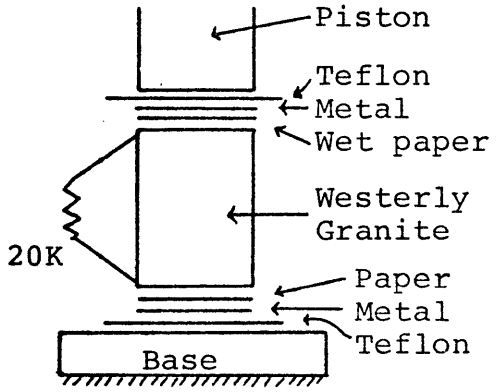

a) lead sheet
b) lead sheet + wet layer
c) copper sheet
d) copper sheet + wet layer

The wet layer of paper is included to ensure better electrical contact to the rock. Results tend to be inconsistent, because as the paper dries, the resistance increases. The copper was annealed before testing to reduce

strain hardening effects, and enable the sheet to conform better to the rock surfaces. However, as the copper is stress cycled many times, strain hardening can become permanent, even after annealing. The electrical conduction properties of the copper lattice will vary slightly because of distorted grains and dislocation pile-ups. This effect will also cause the material to become less pliable.

There appeared to be no significant frequency dependance with the various electrode combinations, however both the wet and dry copper in the stress test showed higher resistance values than the correct value of 20 kilohms $\pm$ 200 ohms (Figure D1).

The dry lead sheet was chosen as the electrode material. Lead is able to conform better to the surface of the sample than the copper sheet, due to its low yield stress. This is particularly important when testing sandstones, which can have a very course surface. There was no apparent stress effect with the dry lead.

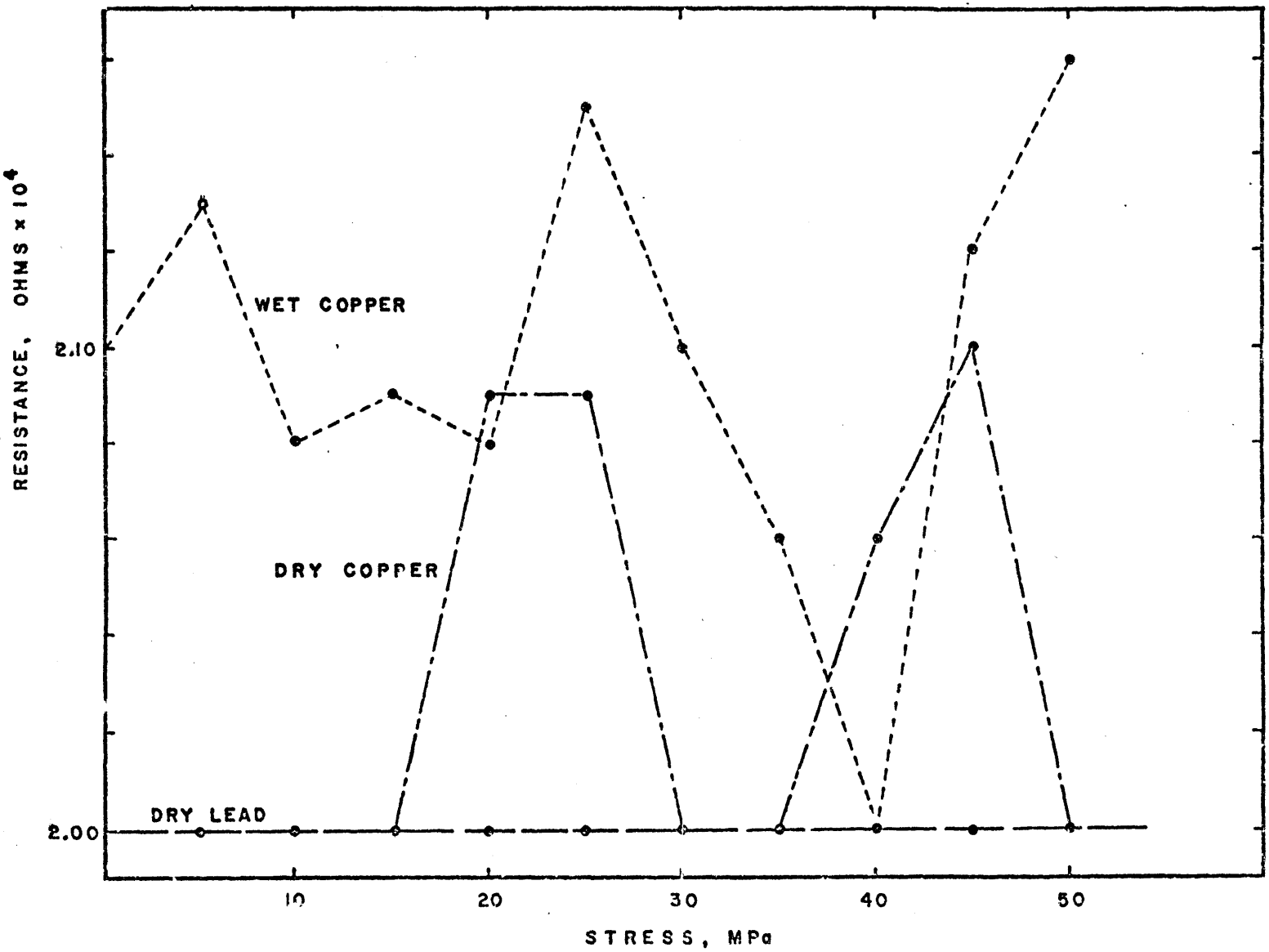

Figure D1 Stress effect of various electrodes, 20K resistor at 10 HZ

APPENDIX D3

Frequency Effects

When dealing with high impedance rocks, second order effects become important. This is particularly true over the frequency spectrum. Consider a dry or partially saturated rock between two copper wires. Because the rock is so much less conductive than the wires, it has some of the characteristics of a capacitor. A model of the system could be represented as shown below.

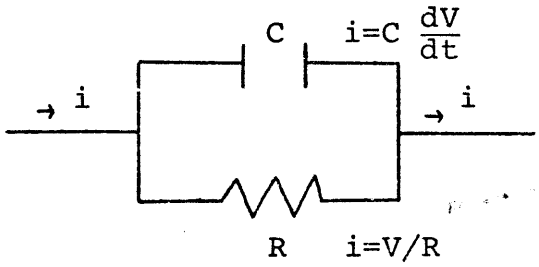

Since the current through the capacitor i=dV/dT C, then at high frequencies, dV/dT will be large. As the current through C increases with higher frequencies, there is correspondingly less current through R. The meter reads a smaller voltage across R, and hence a smaller R than the true value. The actual response can be found by analyzing $Z_R || Z_C$.

$$Z_R = R$$

$$Z_C = \frac{1}{jfC}$$

$$\frac{1}{Z} = \frac{1}{R} + jfC = \frac{1 + jfCR}{R}$$

$$Z = \frac{R}{1 + jfCR}$$

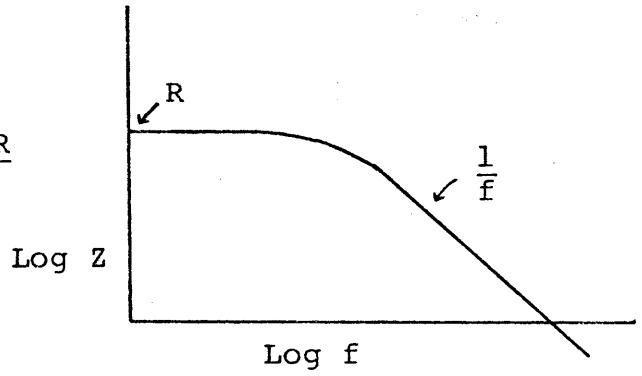

When the frequency is small, Z=R, and when the frequency is large Z falls off as $1/\omega$. There will be a family of curves for varying resistance.

The accuracy of standard film resistors at 10^7 ohms breaks down at 100 Hz, therefore a frequency of 10-100 Hz is suitable to eliminate the capacitance effects of the fixed resistors in the electrical resistance bridge of method 3.

The plot in Figure D2 was obtained using rocks of varying saturation with no axial stress. The tuffs have a high internal capacitance. Since the point of this experiment is not to investigate the frequency dependance of resistance in the tuffs, it is necessary to run the frequency as low as possible to measure the high impedance samples. Above 10^7 ohms (at 10 Hz), the resistance values are already on the sloping part of the response curve. Thus they represent a minimum resistance, and are a contributing

factor to the scatter in the data. Frequencies of less than 10 Hz are not desirable due to the electrolyzing problems of a DC-like current.

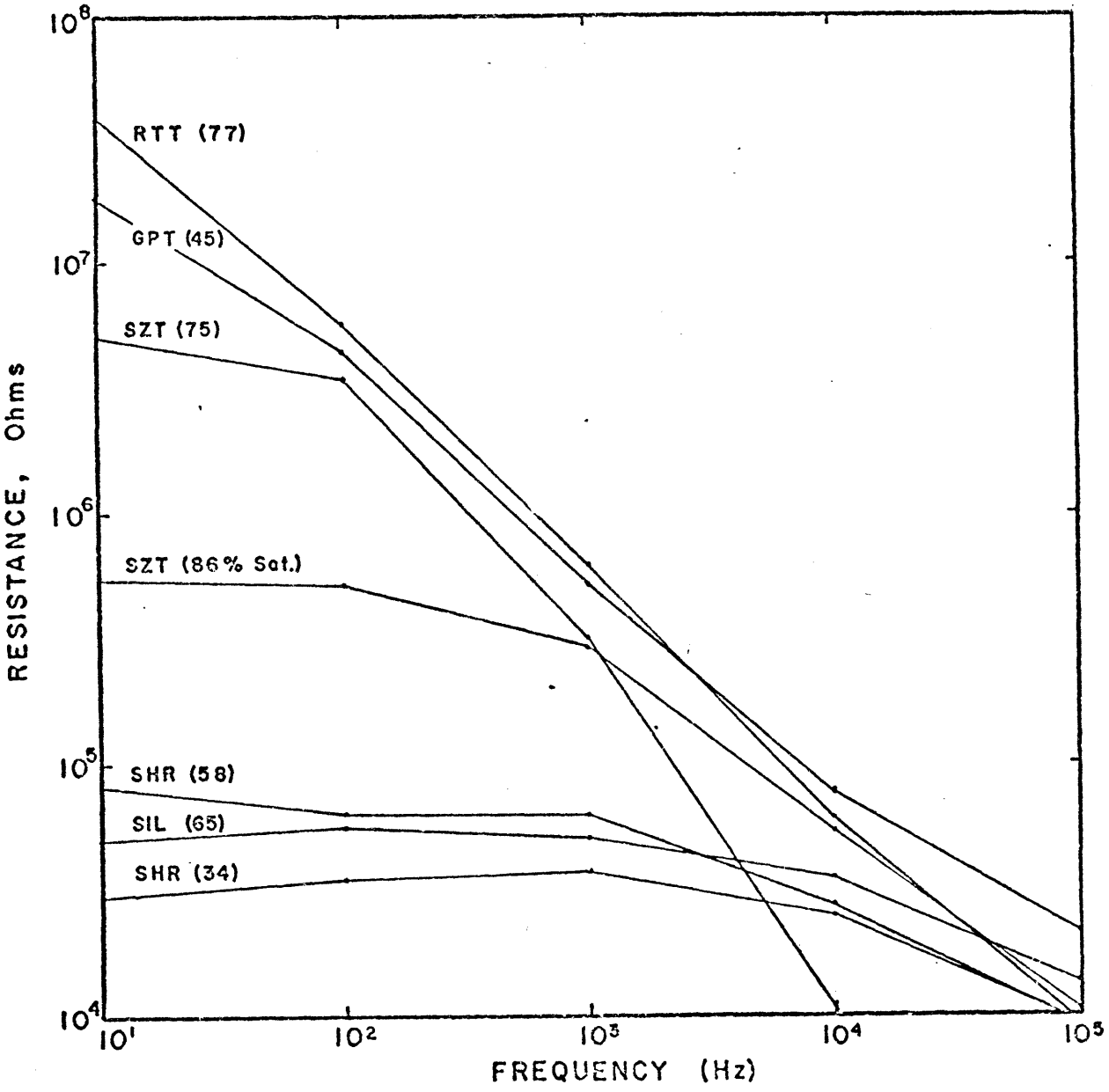

Figure D2 Resistance fall-off with frequency for the California tuffs at varying saturations

REFERENCES

Brace, W.F., Electrical resistivity of sandstone Final report to Defence Nuclear Agency, contract no. DNA-001-74-C-0057, 40p, 1974

Brace, W.F., Permeability from resistivity and pore shape, J. Geophys. Res., 82(23), 3343, 1977

Brace, W.F., and A.S. Orange, Electrical resistivity changes in saturated rocks during fracture and frictional sliding, J. Geophys. Res., 73(4), 1433, 1968

Brace, W.F., A.S. Orange, and T.M. Madden, The effect of pressure on the electrical resistivity of water saturated crystalline rocks, J. Geophys. Res., 70(22), 5669, 1965

Carozzi, A., Microscopic Sedimentary Petrology John Wiler & Sons, Inc. New York, 1960

Madden, T.M., Electrical measurements as stress-strain monitors, U.S.G.S. Office of Earthquake Studies. Proceedings of conference VII: Stress and strain measurements related to earthquake prediction. Open file report 79-370; Menlo Park, California, 1978

Parkhomenko, E.I., Electrical Properties of Rocks Plenum Press, New York 314p, 1967

Rikitake, T. and Y. Yamazaki, Electrical conductivity of strained rocks: The fifth paper. Residual strains associated with large earthquakes as observed by a resistivity variometer. Bul. Earthquake Res. Inst. 47, 99, 1969

Sprunt, E.S., and W.F. Brace, Direct observation of microcavities in crystalline rocks, Rock Mechanics and Mining Sciences and Geomechanics Abstracts, 11(4), 139, 1974

Stesky, R.M., and W.F. Brace, Electrical conductivity of serpentinized rocks to 6 kilobars. J. Geophys. Res., 78(32), 1973

Yamazaki, Y., Electrical conductivity of strained rocks: The first paper. Laboratory experiments on sedimentary rocks. Bul. Earthquake Res. Inst. 43, 783, 1965

Yamazaki, Y., Electrical conductivity of strained rocks: The second paper. Further experiments on sedimentary rocks. Bul. Earthquake Res. Inst. 44, 1553, 1966